NASA CR-135258

(NASA-CR-135258) THE EFFECT OF ENVIRONMENTAL PLASMA INTERACTIONS ON THE PERFORMANCE OF THE SOLAR SAIL SYSTEM Contractor Report, Jul. 1976 - Jul. 1977 (Maya Development Corp., San Diego, Calif.) G3/33

N78-13325

HC A06/MF A01

Unclas 53644

THE EFFECT OF ENVIRONMENTAL PLASMA INTERACTIONS ON THE PERFORMANCE OF THE SOLAR SAIL SYSTEM

M. Douglas, R. LaQuey and S. DeForest

MAYA DEVELOPMENT CORPORATION

Prepared For

NATIONAL AERONAUTICS AND SPACE ADMINISTRATION

NASA Lewis Research Center

Contract NAS 3-20119

1. Report No.	2. Government Accession No.	3 Recipient's Catalog No
NASA CR-135258		

4. Title and Subtitle	5 Report Date
THE EFFECT OF ENVIRONMENTAL PLASMA INTERACTIONS ON THE PERFORMANCE OF THE SOLAR SAIL SYSTEM.	AUGUST 1977
	6 Performing Organization Code
7. Author(s) MARVIN DOUGLAS, ROBERT LAQUEY AND SHERMAN DEFOREST	8 Performing Organization Report No
	10. Work Unit No YOS 7278
9. Performing Organization Name and Address MAYA DEVELOPMENT CORPORATION 11675 "H" Sorrento Valley Road San Diego, California 92121	11. Contract or Grant No NAS 3-20119
	13 Type of Report and Period Covered Contractor Report July 1976 - July 1977
12. Sponsoring Agency Name and Address National Aeronautics and Space Administration Lewis Research Center Cleveland, Ohio	14. Sponsoring Agency Code

15 Supplementary Notes

16. Abstract

Interaction between the Solar Sail and the natural plasma environment have been examined for deleterious impacts upon the operation of the sail and its associated payload. Electrostatic charging of the sail in the Solar Wind and in near earth environment are examined. Deployment problems are studied. An analysis of electromechanical oscillations coupling the sail to the natural plasma is performed.

As a result of these studies we conclude that none of these effects will have a significant negative impact upon the sail operation. The natural environment will be significantly perturbed and this will preclude measurements of electric and magnetic fields from an attached payload.

17. Key Words (Suggested by Author(s))
Solar Sail
Plasma Interaction
Spacecraft Charging

18. Distribution Statement
Publicly Available

19. Security Classif. (of this report)	20. Security Classif. (of this page)	21. No. of Pages	22. Price*
Unclassified	Unclassified	111	

* For sale by the National Technical Information Service, Springfield, Virginia 22161

TABLE OF CONTENTS

LIST OF FIGURES

LIST OF TABLES

SUMMARY

An attempt has been made to identify possible interactions between the Solar Sail and the natural plasma environment which might have deleterious effects on the operation of the sail or its associated payload. We have attempted to take conservative estimates of possible effects. In all cases, we have tried to report an upper bound to possible interactions.

The net conclusion is that nothing we have found in the environment will preclude safe operation of the Solar Sail. However, the sail itself will perturb any natural environment sufficiently that observations of electric and magnetic fields from an attached payload will not be possible. Similarly plasma composition and low energy particle fluxes will be severely affected. In some cases, even optical observations of objects remote from the sail will be compromised.

EMI induced by the plasma-sail interactions now seems to be much smaller than what had originally been thought.

Electrical-mechanical oscillations induced by the plasma also seem to be smaller than the original analysis had indicated. However, the completely rigorous treatment of this potential problem is beyond the scope of this report. We recommend further study be conducted on this problem. Of particular interest for operation in the near earth environment will be a rigorous analysis of the interaction of the sail with natural plasma waves such as the Pc4 events.

1. INTRODUCTION

The purpose of this report is to assess the interaction between the Solar Sail and the plasma environments which will be encountered in various missions in order to identify any deleterious affects upon the performance of the Solar Sail System. In addition we examine deployment problems due to static electricity since these fall naturally into a general analysis of the electrostatic properties of the Solar Sail. Our approach is both qualitative and quantitative, with an emphasis upon worst case engineering analysis. We are looking for the "show stoppers", those critical problems which can cause a major system failure. A wide range of problems is covered, in as much depth as time has allowed. Areas needing further study are indicated, as is our present state of understanding.

We begin by examining the solar wind environment. Satellite data is used to develop a model of the solar wind which can then be used to determine the voltage to which a Solar Sail might be expected to charge. The environmental definition is done from the perspective of spacecraft charging. Thus when parameter choices involving judgement must be made, we shall always make choices between observed parameters which tend to give the largest value for the electron temperature, as this quantity determines the voltage to which the spacecraft will charge, and we prefer to overestimate rather than underestimate this voltage.

Having defined the solar wind environment we then proceed to perform an analysis of the electrostatic charging of the Solar Sail by the solar wind. The first and most important problem addressed is differential charging. We examine the possibility of developing large potential drops across the various regions of the spacecraft body, with the possibility of high voltage breakdown. A second consideration is the disturbance of the plasma environment about the sail, and how this disturbance affects measurements of this environment.

We next examine the use of the Solar Sail in the near earth environment. Again a general charging analysis is performed. Electromechanical effects (resonant interaction with PC4 oscillations) specific to this environment are examined.

Electrostatic forces acting upon the sail arise from the environment and from frictional effects or contact potentials. These latter are important during deployment, which represents a special case for analysis. An assessment of the minimum forces anticipated is performed, as part of a worst case analysis of the deployment problem.

Another problem arises from the forces associated with electrostatic charging by the environment. Electromechanical oscillations arise from the coupling of waves on the sail to the surrounding plasma. We have analyzed this problem in an attempt to determine if the interaction with the solar wind

will cause unstable oscillations of the sail. Several cases are examined and dimensionless parameters characterizing potential instabilities are developed.

The existence of plasma flow across a magnetic field in the solar wind gives rise to still another force, the induction force. This force and a corresponding induction current are analyzed to determine their impact upon sail performance. The modification of the photo electron sheath by these forces is examined.

For the Solar Sail to be useful it must transport a payload. We examine the effects of Solar Sail operation upon the payload. Areas of concern are: 1) safety, 2) effects on particle measurements, 3) effects on field measurements and 4) electromagnetic interference (EMI). Early concerns with EMI have lessened substantially as the magnitude of the sail charging problem became better understood but we mention it for the sake of completeness.

The need for experimental work is indicated in a final section. A few simple experiments might be especially useful in assessing the problems associated with static electrification during deployment.

2. THE SOLAR WIND ENVIRONMENT

The solar wind is a supersonic predominantly electron-proton plasma flowing approximately radially outward from the sun. It is generated by the expansion of the solar corona. Between r = .3 a.u. and past 1.0 a.u. the density n varies approximately as $1/r^2$, the flow velocity V is approximately constant. These statements however describe only the time average behavior. In fact very large fluctuations are normal. They are due in part to the fact that there is continuous activity near the base of the corona and that the corona has important structure which rotates with the sun (e.g. coronal holes). Thus present understanding of the solar wind recognizes the existence of high speed particle streams emanating from coronal holes, and shock fronts which build up when fast plasma overtakes cold plasma. For this reason our environmental specification will rely on satellite data. The vast bulk of the observations are at 1.0 a.u. [1,2,3] and there do exist theoretical models [4] which allow extrapolation to .3 a.u. We shall examine this scaling as well as make use of the limited data at .3 a.u. that we have been able to locate on Helios [5] satellite observations. The quantities we require are the flow speed, density and electron and proton temperatures. Since the distribution functions are not isotropic Maxwellians some interpretation of experimental data is required. In the

following we shall always make choices between observed parameters that tend to give the largest value for the electron temperature, as this quantity determines the voltage to which a spacecraft will charge, and we prefer to overestimate rather than underestimate this voltage.

a. Distribution Functions

Figure 2.1 illustrates recent data [5] on proton temperature, flow speed and density from 1.0 a.u. to .3 a.u. Flow velocities as high as 800 km/sec are evident. The average density behaves as $n \propto 1/r^2$. The peak density near .3 a.u. is about $300/cm^3$, and we shall use this as the most extreme condition for charging calculations; $100/cm^3$ would be a good average value. From the proton temperature we wish to deduce a value of the electron temperature. The scaling calculations of Ref. 5, see Figure 2.2, seem to indicate about a 20 - 30% change in electron temperature between 1.0 a.u. and .3 a.u. Figure 2.1 indicates a roughly similar change in the maximum proton temperature. We have not been able to locate electron temperature data from Helios and are not sure that it has been published yet. We shall assume that the more thoroughly investigated properties of the proton and electron distributions at 1.0 a.u. hold at .3 a.u., and make use of the most extreme electron temperature that can be deduced in this manner. Figure 2.3 shows a plot of electron and proton temperatures at 1.0 a.u. observed with the Vela 4 satellite.

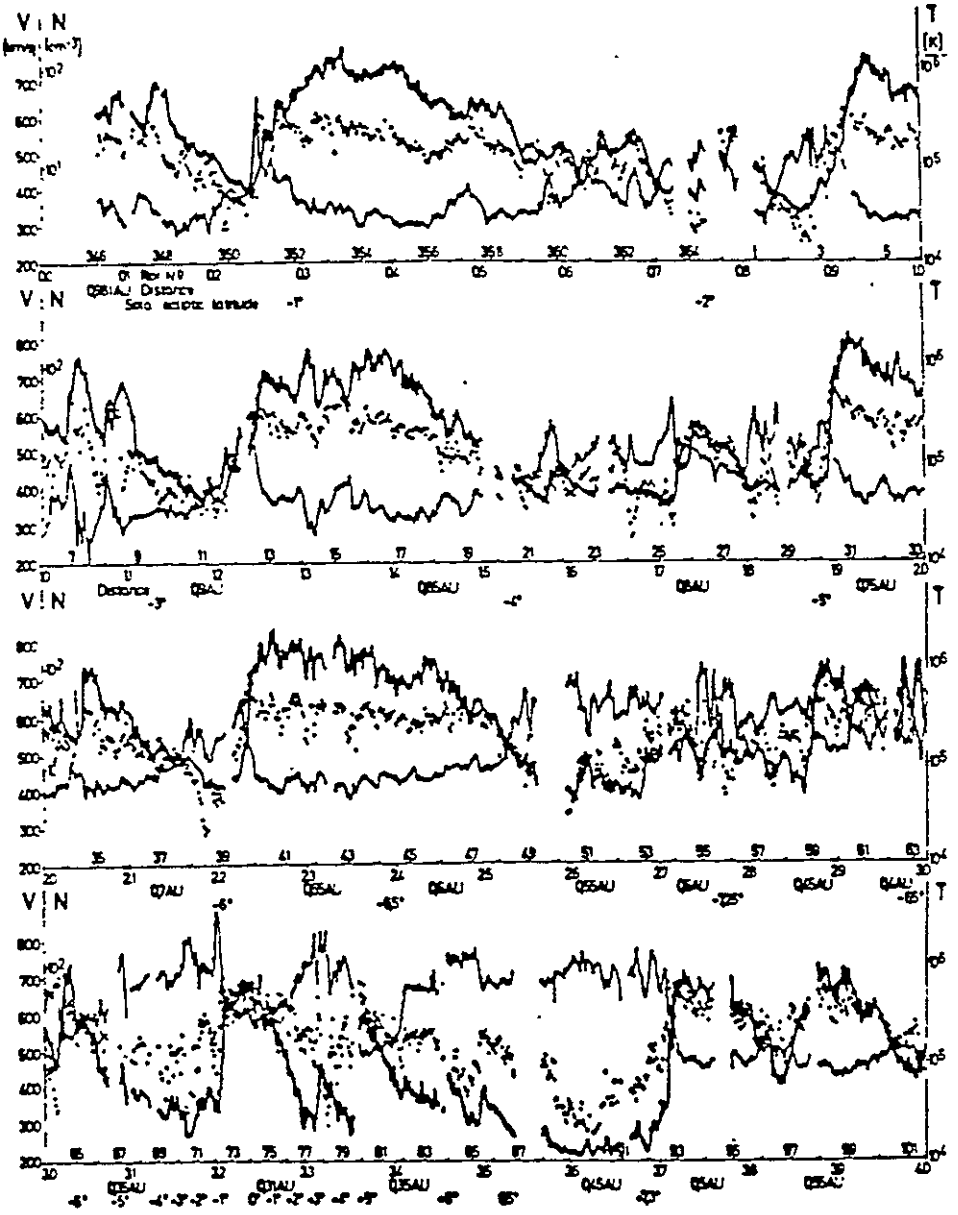

Figure 2.1. Solar wind bulk velocity (heavy line), density (thin line), and temperature (dotted line) as measured by Helios A (Ref. 5).

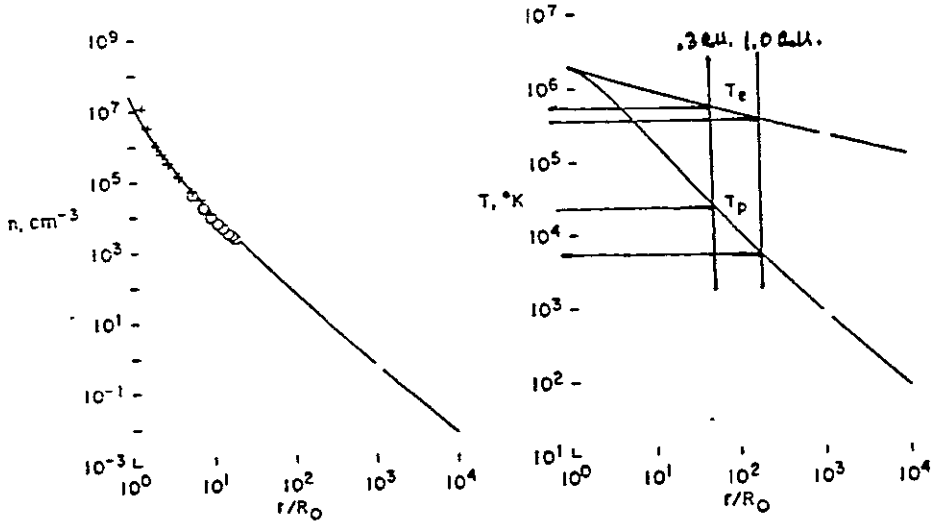

Figure 2.2. Temperature and density variation with radius (Ref. 4).

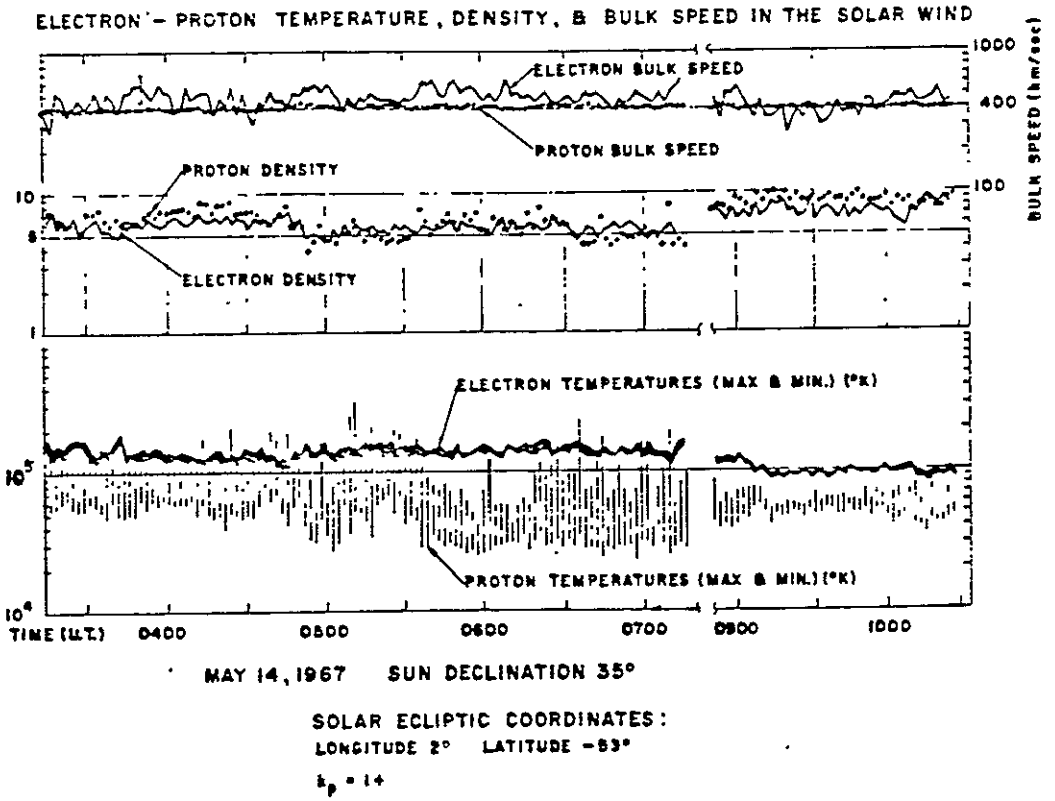

Figure 2.3. Solar wind parameters at 1.0 a.u. (Ref. 1).

The maximum and minimum values of the proton temperature, T_{max} and T_{min}, reflect the anisotropy of the distribution with respect to the magnetic field direction. For our purposes we can take the electron distribution as isotropic, and according to Figure 2.3 we can take the electron temperature to be the maximum proton temperature. The proton distribution is fairly well represented as an anisotropic Maxwellian. The proton anisotropy ratio is given by $K = T_{max}/T_{min}$ and at 1.0 a.u. it ranges from 1.1 to 3.4 in the data of Ref. 2. The average temperature that is typically constructed is defined as

$$T = 1/3\ (T_{max} + 2T_{min}) = 1/3\ T_{max}\ (1 + \frac{2}{K}).$$

Figure 2.3 indicates values $T_{max} \sim 1.5 \times 10^5\ ^\circ K$, and $T_{min} \sim 5 \times 10^4\ ^\circ K$, or $T \sim 8.3 \times 10^4$. This is somewhat lower than the value of $\sim 3 \times 10^5\ ^\circ K$ apparent in Figure 2.1. We shall proceed on the assumption that $3 \times 10^5\ ^\circ K$ represents the average temperature T at 1.0 a.u., noting that the bulk speeds observed in the Helios data are considerably higher than that shown in the Vela data, and that increasing V is correlated with increasing proton temperature[2]. Identifying T_e with T_{max} and using the maximum value of K we find

$$T_e \sim \frac{3T}{1+2/K} \leq 2T\ .$$

The average proton anisotropy increases with radius because the magnetic moment $W_\perp/B$ is constant and B is decreasing. This being the case it appears that taking $T_e \sim 2T$ should be a safe upper limit on the electron temperature. From Figure 2.1

at .3 a.u. we find then T ~6×10^5 °K at maximum, and thus $T_e \leq 1.2\times10^6$ °K. We thus have deduced so far the extreme plasma parameters

$V \sim 300 - 800$ km/sec

$n \sim 100\text{-}300/cm^3$

$T_e \leq 1.2\times10^6$ °K

$T \sim 6\times10^5$ °K

$T_{max} \sim 1.9T = 1.14\times10^6$ °K

$T_{min} \sim .55T = 3.3\times10^5$ °K.

Several comments are in order.

1) The proton temperature is not too important for charging calculations because the proton directed velocity is large compared to thermal velocity.

2) The observations illustrated in Figure 2.1, 2.2 were made during periods of low average solar activity. We have not located corresponding data on active periods for comparison. If any problems were found with solar wind spacecraft charging it would be important to make a more thorough study.

3) No data is available for high solar latitude (beyond ~10°). Various models indicate variations by factors of order 2 for quiet conditions (6).

The Electron Distribution

It is important for charging calculations to recognize that although the electron distribution is approximately isotropic it is not a single Maxwellian. It can be adequately represented as the sum of a cold or "core" Maxwellian which contains the bulk of the electrons, and a hot or "halo" Maxwellian. Reference 3 gives values for the number of hot electrons to total N_H/N_H+N_c ranging from $.038\pm.017$ to $.071\pm.028$, and the temperature ratio

$$R_T = T_H/T_c = \frac{8\times10^5\ ^\circ K}{1.25\times10^5\ ^\circ K} = 6.4 \quad .$$

We assume this ratio holds at .3 a.u. and identify T_e with the average temperature

$$T_e = \frac{N_c T_c + N_H T_H}{N_c + N_H} = T_c \left\{ \frac{N_c + R_T N_H}{N_c + N_H} \right\} = 1.54 T_c$$

using $N_H/N_H+N_c \sim .1$, the maximum value.

We find

$$T_c = T_e/1.54 = 7.79\times10^5\ ^\circ K = 67.2 \text{ eV}$$

$$T_H = R_T\ T_c = 5\times10^6\ ^\circ K = 431 \text{ eV}$$

We shall use these to characterize the electron distribution.

In Ref. 5 a new feature of the solar wind electrons was suggested. This is that the halo electrons are actually the scattered portion of an electron beam component of the solar

wind. The halo electrons appear to have roughly the same energy as the observed beam component. We shall not attempt to incorporate this new feature into our charging estimates but work with the more conventional two temperature Maxwellian. Thus for the electron distribution we take

$$f_e = n \left\{ .9 f_m(T_c) + .1\ f_m(T_H) \right\} \quad ,$$

where $f_m(T)$ is the normalized Maxwellian characterized by temperature T. In f_m we neglect the flow speed because it is small compared to thermal speed for electrons.

3. SAIL CHARGING IN THE SOLAR WIND

The interaction of a spacecraft with the ambient plasma is an important consideration for a number of reasons. The first and most important of these is the possibility of developing large potential drops across various regions of the spacecraft body, with the possibility of high voltage breakdown. This could lead to electromagnetic interference with consequent electronic malfunction and possibly permanent damage. In the case of the solar sail breakdown occuring in the kapton sail film could lead to premature degradation of the sail itself. A second common consideration is the disturbance in the ambient electric and magnetic fields and particle environments produced by the spacecraft, and how measurements of these environments are affected. To give any final answer to this question would require more detailed analysis than could be provided in the term of this study; we have provided a short section suggesting a few possible effects of the sail on payload operation. It is true that plans call for jetissoning the sail before encounter with Halley's comet, in which case the problem becomes a more conventional one. On the other hand the cranking orbit offers a unique opportunity to examine the solar wind at all latitudes; data at present exists for only a few degrees out of the eliptic.

Summary. The charging characteristics of the sail depend strongly on whether or not the front (sunny) side and

rear (shady) side are electrically shorted together. If disconnected the front side should float at some 1-10 volts positive with respect to space and the rear side could float to 300 volts negative. The shorted sail should float at 1-10 volts positive, a safe and desirable situation. The small positive potentials result because of large fluxes of photoelectrons that are emitted and the proton flux from the directed flow of solar wind. For heliogyro blade surfaces near parallel to the solar wind these factors are greatly reduced and large negative potentials (-200 to -400 volt) could develop over the whole blade. We have analyzed this possibility and find it unlikely that this could occur. If all blades were shorted together it would be virtually impossible.

Spacecraft charging and wake. When imbedded in a plasma a spacecraft floats to a potential $\varphi = \varphi_s$ such that the various currents to the spacecraft surface, which are all functions of φ, sum to zero. The major current contributors are plasma electrons minus associated secondaries, plasma protons plus associated secondary electrons, and photoelectrons emitted from sunlit surfaces.

The sail is imbedded in the flowing solar wind plasma. The dynamics of this plasma is dominated by the flow velocity of the protons (which are the dominant ion constituent). The protons are supersonic, that is the flow velocity

$V >> V_p = \sqrt{\frac{2kT}{m_p}}$, the proton thermal velocity (V/v_p = M∿4-10). On the other hand typically $v_e = \sqrt{\frac{2kT}{m_e}} >> V$, however we shall consider the possibility that in some circumstances v_e does not exceed V by a huge amount. Under these conditions (M>>1) a cavity is formed in the plasma behind the spacecraft. There are two major factors affecting the dynamics of this cavity. If all ions had precisely velocity $\vec{V}$ and the ones hitting the sail were perfectly absorbed a cylindrical cavity whose cross section was that of the sail frontal cross section would form, Figure 3.1. The ion thermal spread gives the average ion a velocity component v_p in the transverse direction. This alone would cause the cavity to fill in a distance downstream $b \sim (v_p/V)\frac{W}{2}$, where W is the smallest transverse sail dimension. Aside from ion thermal effects the wake will fill in due to plasma electric fields. These fields come about for two reasons, 1) the electrons being much faster than the ions tend to drag them into the cavity (ambipolar field), 2) the spacecraft surface is typically charged to some potential, which also influences the trajectories.

The problems of theoretically calculating the structure of the disturbed plasma (frequently referred to as the wake) moving around a body in space requires solving a complicated system of coupled nonlinear partial integro-differential equations. The equations consist of the Vlasov (collisionless Boltzmann) equation for the ions and electrons, and the Poisson

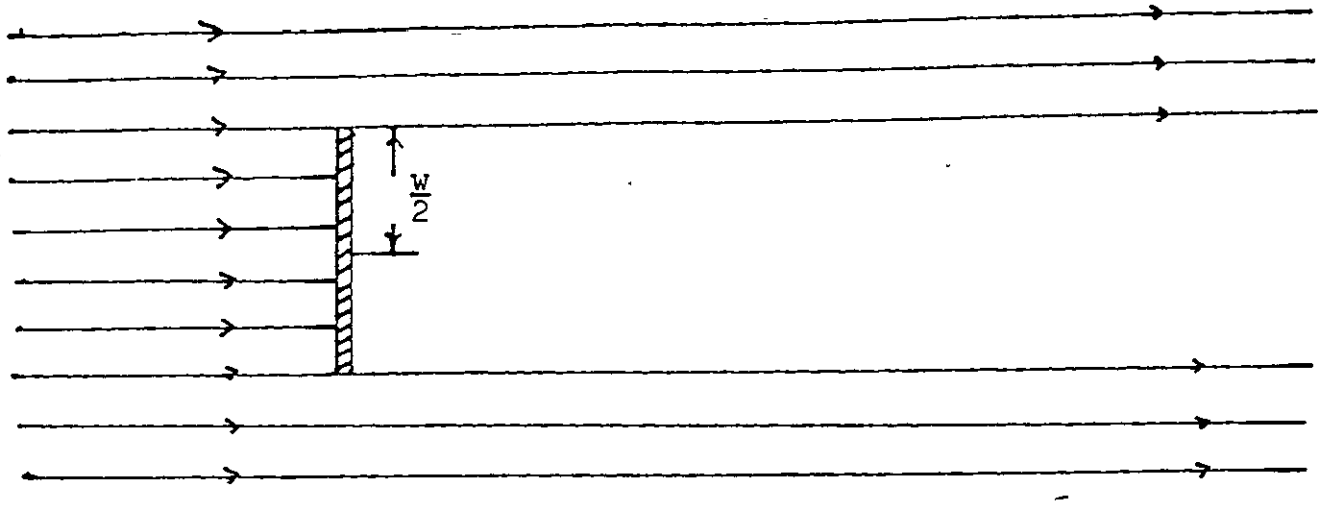

Figure 3.1(a). Ion trajectories with no thermal dispersion.

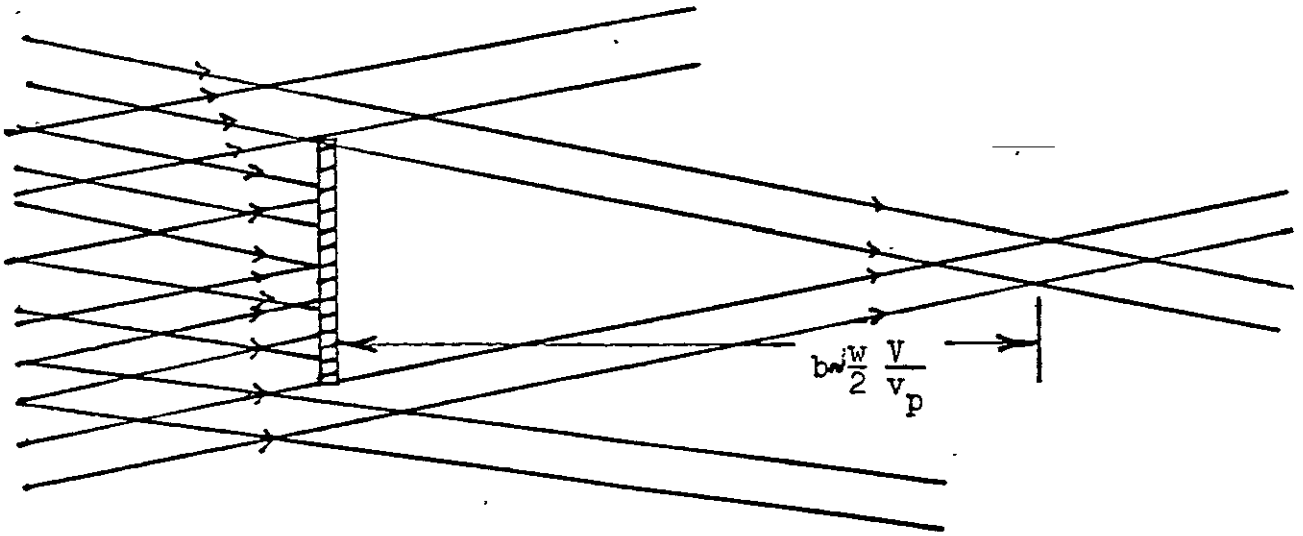

Figure 3.1(b). Filling in of cavity due to thermal dispersion.

equation relating the electric field to the particle distributions. The final solution must give zero electric current to the spacecraft, which means that its surface potential must be self-consistently included. Since such a calculation was well beyond the scope of this study we have resorted to an examination of the literature to determine if some useful physical information could be extracted. We have concentrated on those factors which would be important for the charging of the sail. That is we have attempted to extract information about electric currents to the sail independent of detailed wake morphology.

There have been numerous calculations of the wake of a large spacecraft. These are reviewed in References 1-6. In none of these have we found any discussion of plasma properties exactly at the rear surface of the spacecraft. Many of the calculations have in fact been carried out for planar surfaces (in the limit of large Mach number M the calculations for an arbitrarily shaped body reduce to those for a disc with the shape of the body frontal cross section). Typically approximations are made which are simply wrong near the rear surface. We feel it is still possible to obtain a useful estimate of the plasma current to the rear surface.

The largest particle flux in the plasma is the electron flux, because they are travelling much faster than the protons. In the absence of photoemission this causes the spacecraft surface to come to a potential $\mathcal{G}_s$ which is negative. In this circumstance the electron current density to a surface element

under quite general conditions is the sum of

$$\Gamma_e(\varphi_s) = \Gamma_{eo}\, e^{\frac{e\varphi_s}{kT}} \quad , \quad \Gamma_{eo} = \frac{n}{2\sqrt{\pi}} \sqrt{\frac{2k\bar{T}_e}{m_e}}$$

for each Maxwellian component of the electron distribution at infinity. This expression will be reduced on concave regions of the body surface since some current producing trajectories coming in from infinity are cut off by the body. For the solar sail geometry, and in particular the heliogyro, this should be a negligible factor. If there exists a potential well (electron surplus) astride the trajectories leading to the surface element in question this too will reduce the above expression since the electron potential energy function will have a hill. For a disc shaped spacecraft whose radius is less than five Debye lengths λ_D such wells apparently do not exist (4), although they certainly could behind the square sail since the square sail is some 80-250 Debye lengths wide. We shall be focusing on the heliogyro. For it the blade width w is anywhere from $.5\lambda_D$ to $5\lambda_D$ depending on solar distance and conditions. The work that we have examined for infinitely long blade like configurations (6) indicates that shallow potential wells may exist. These calculations may not be definitive however since the ion thermal velocity spread was neglected, and they seem hard to reconcile with the disc results of Ref. 4. Since potential wells <u>reduce</u> the electron flux[4] we feel it is

prudent to use the electron current calculated as if they did not exist, that is $\Gamma_e(\mathcal{V}_s)$. This will give a worst case value for the negative potential on the rear of the unshorted sail. If the sail is positive the electron flux will be increased over simply the surface integral of Γ_{eo}. For example if a positively charged plasma probe is cylindrical in shape its effective collection area is $\sqrt{1 + \frac{e\mathcal{V}_s}{kT_e}}$ times its actual area, and we might expect a similar effect to hold for a bladelike probe. Since the positive potentials we shall find are typically just a few volts $e\mathcal{V}_s/kT_e << 1$ we shall take the enhancement factor to be unity. This has the effect of overstating small slightly positive potentials which are not serious for sail operations anyway.

It is reasonable in our estimation to take the ion flux to the rear of the sail to be simply zero. For an uncharged sail it requires protons moving towards the sun to hit the rear of the sail, and these are a very small fraction for solar wind Mach numbers M. Figure 3.2 shows surfaces of constant ion concentration behind a semi-plane. The ion density is clearly falling rapidly as the rear surface is approached. For a negatively charged rear surface additional ions will be attracted by the electric field. These will tend to reduce the field. Thus it should be a good first approximation to neglect these ions. We shall use the leakage current through the kapton to

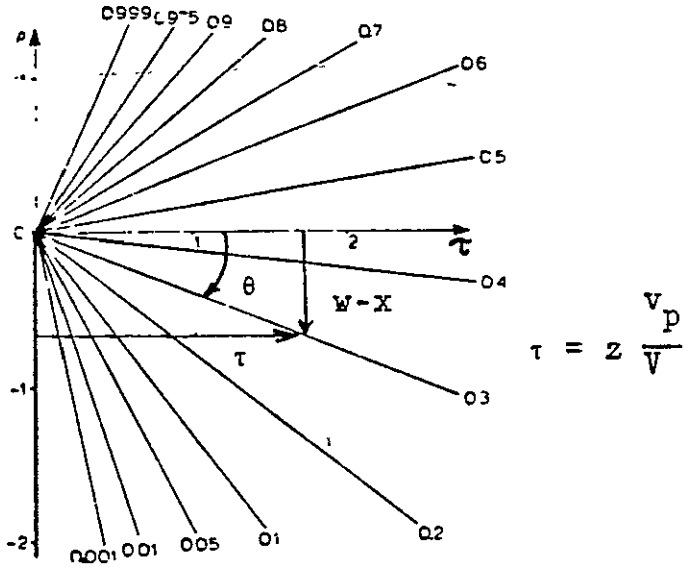

Figure 3.2(a). Surfaces of constant concentration near corners of a semi-plane (Ref. 3).

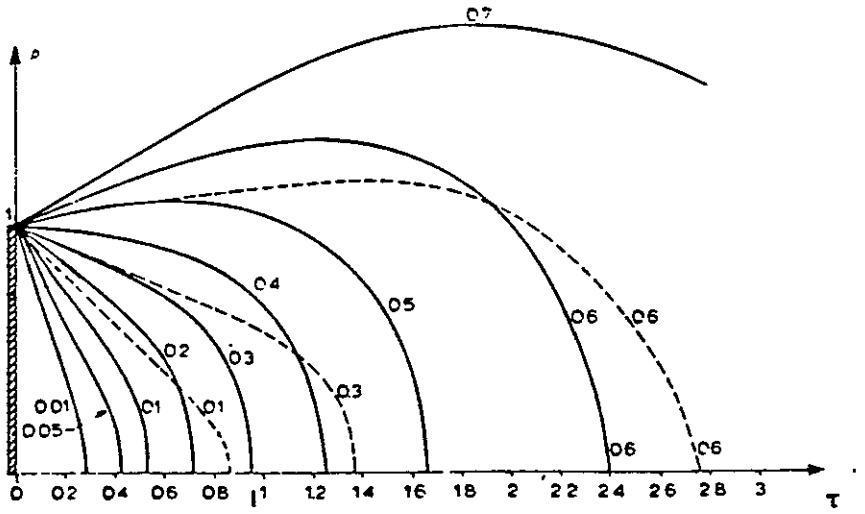

Figure 3.2(b). Surfaces of constant relative concentration n/n_o for flow past a plate. The dotted lines correspond to free motion of ions (zero electric field) (Ref. 3).

balance the electron current. In one sense this is academic. The presence of large negative rearside potentials is undesirable enough, and its remedy, the shorting together of front and rear, simple enough that it almost certainly will be done. On the other hand the rear side is vulnerable to any proton fluxes that may exist because its metallic coating is only 50-100 Å thick. Calculations have suggested that the plasma behind the body is unstable[3,7] and this could cause particles to be heated and deflected to the rear surface. In Figure 3.3 are illustrated the proton distribution function as a function of angle from the sail edge, showing that it becomes beamlike, and the calculated region of instability. We do not know if such instability will be important.

In summary we shall be using Γ_{eo} for positive surfaces, $\Gamma_e(\mathcal{V}_s)$ for negative surfaces, and the proton flux to be calculated in the following for the front of the sail. We shall be neglecting the potential gradient that exists along the sail surface due to the electric field induced by the VxB of the plasma (Section 7).

Plasma Currents to Sail. The external currents we shall take into account are plasma protons, plasma electrons, photoelectrons, and a rough estimate of secondary electrons due to electron impact.

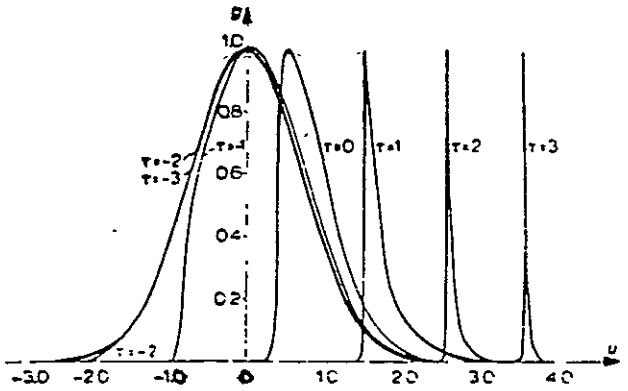

$$\tau = M \tan \theta$$

$$= \frac{V}{v_p} \frac{w/2 - x}{z}$$

$$u = \frac{V}{v_p}$$

Figure 3.3(a). The ion distribution function $g(u,\tau)$ for various values of velocity angle with respect to solar wind direction (Ref. 3, 7). See Figure 3.1 for coordinates.

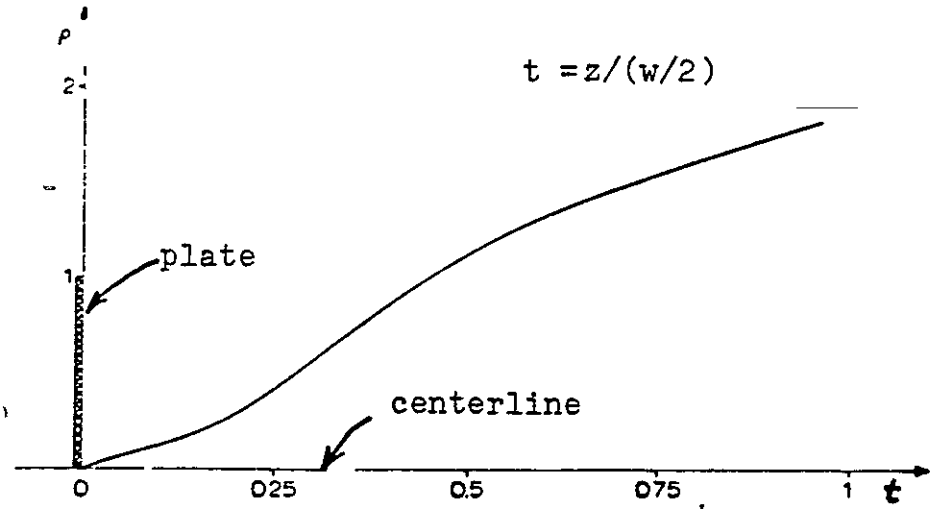

Figure 3.3(b). The boundary of the region of instability for flow past a plate (Ref. 3, 7). Ion acoustic waves are unstable in the region above the curve.

1) Plasma Protons: The proton distribution function is taken as a Maxwellian with different temperatures parallel and perpendicular to the magnetic field $\vec{B}$ which are on the order of 10^5 ^oK but can extend higher (see Section 2). We assume that B and the directed flow velocity lie perpendicular to the plane of the sail (it will turn out that this does not matter). The distribution function is thus

$$f_p(v_x,v_y,v_z) = n\left(\frac{m_p}{2\pi kT_\perp}\right)\left(\frac{m_p}{2\pi kT_{||}}\right)^{\frac{1}{2}} e^{-\frac{m_p(v_x^2+v_y^2)}{2kT_\perp}} e^{-\frac{m_p(v_z-V)^2}{2kT_{||}}};$$

the flux to the sail is

$$\Gamma_p = \int dv_x dv_y dv_z \cdot v_z f_p = n\left(\frac{m_p}{2\pi kT_{||}}\right)^{\frac{1}{2}} \int_{v_{min}}^{\infty} v_z dv_z e^{-\frac{m_p(v_z-V)^2}{2kT_{||}}}.$$

v_{min} is the minimum positive velocity a proton can have and still reach the surface: $v_{min} = 0$ for a surface at zero or negative potential and $v_{min} = \sqrt{\frac{2e\mathcal{V}_s}{m_p}}$ for a positively charged surface. We normalize $\mathcal{V}_s$ to the plasma temperature, defining $\Phi = e\mathcal{V}_s/kT_{||}$. The flux result is

$$\Gamma_p = n\, v_p \left[\frac{1}{2\sqrt{\pi}}\, e^{-(m-\sqrt{\Phi})^2} + \tfrac{1}{2}M(1 + \mathrm{erf}(M-\sqrt{\Phi}))\right].$$

Regarding erf as an odd function includes the case $\Phi > M$. Solar wind proton Mach numbers are of the order M = 5-10. For zero body potential the flux is very well approximated by $\Gamma_{po} = nV$. Thus the amsotropy with respect to B is insignificant. In Figure 3.4 we have plotted the flux normalized to Γ_{po} as a

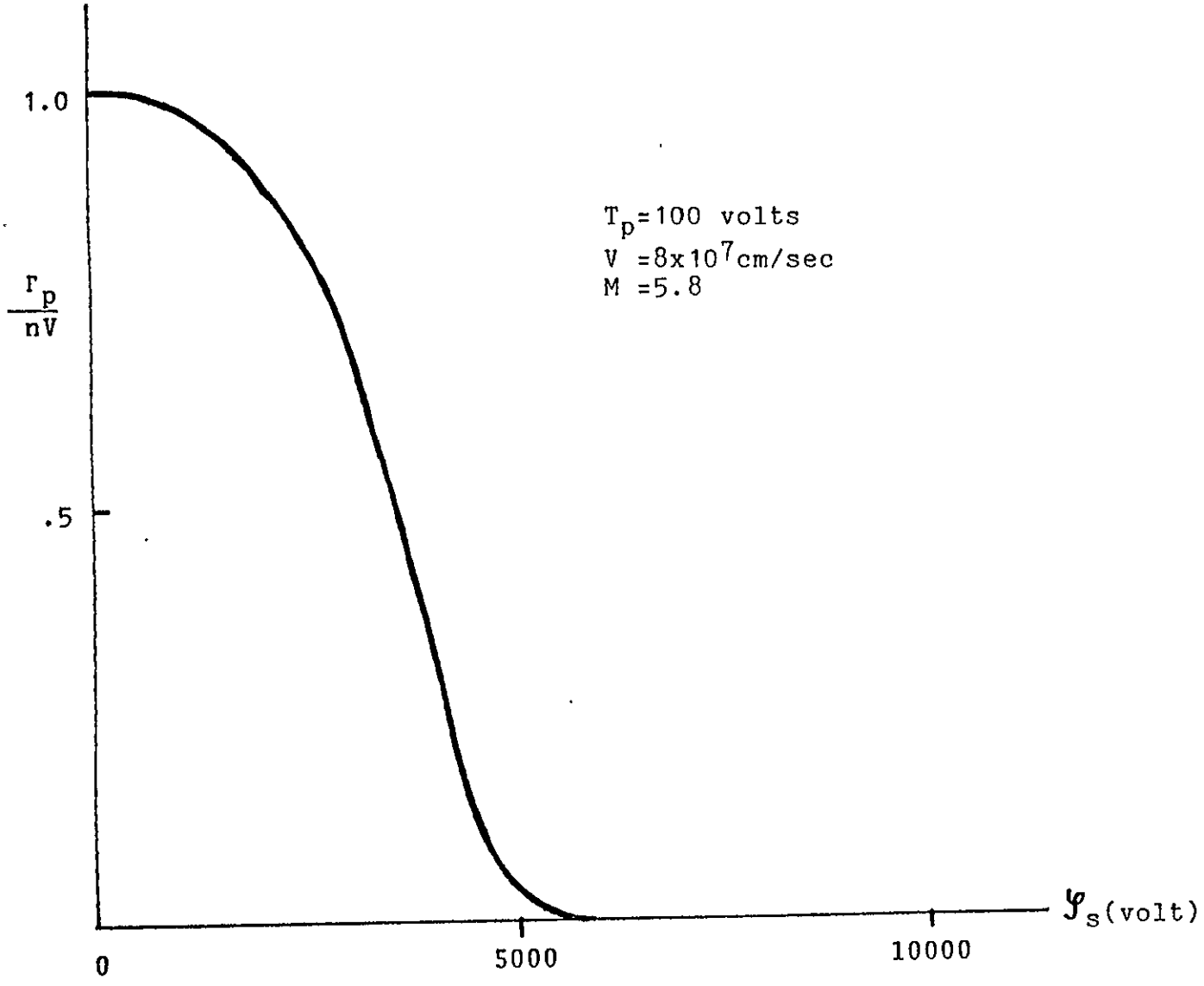

Figure 3.4. Proton flux as a function of positive sail potential.

function of $\mathcal{V}_s$. What this plot shows is that very high positive potentials are required to significantly retard the protons, and Γ_{po} is a good approximation for potentials up to ~1000 volts. Since such high positive potentials are unlikely to be encountered the proton flux we shall use in calculations will be $\Gamma_p = \Gamma_{po}$.

2) Plasma Electrons: The integral calculated above for the protons applies to the electrons. For these M<<1 typically. For M = 0 the electrons fluxes are Γ_{eo}, $\mathcal{V}_s > 0$, and $\Gamma_{eo}\, e^{e\mathcal{V}_s/kT}$, $\mathcal{V}_s < 0$ for each Maxwellian component.

3) Photoelectrons: The charging of a body in space is strongly influenced by photoemission of electrons from its sunlit surfaces. The emitted flux depends on the solar photon energy spectrum and the emitting material. If the body potential $\mathcal{V}$ is positive with respect to that at large distance the flux will also depend on $\mathcal{V}$ because low energy electrons will be attracted back to the surface. Extensive work has been carried out[8] measuring the photoelectron spectrum as a function of incident photon energy. These are then folded in with the solar spectrum and integrated over angles of emission to give the sunlight emission spectrum and current flow from a surface.

The total flux from aluminum at 1.0 a.u. is given as[8] $I_s = 2.6\times10^{10}/cm^2\text{-sec}$, and would be $I_s = 2.9\times10^{11}/cm^2\text{-sec}$ at .3 a.u. The perpendicular energy distribution, shown in

Figure 2.1-d, Ref. 8, can be reasonably well represented as the sum of two Maxwellians

$$f(E) \propto \left(\alpha_1 e^{-E/E_1} + \alpha_2 e^{-E/E_2}\right) ,$$

with $\alpha_1 = 1.1$, $\alpha_2 = .15$, $E_1 = .625$ eV, $E_2 = 2.0$ eV.

The total flux from a positive surface is

$$\Gamma_{ph} = \int_{v_{min}}^{\infty} v(E)\, f(E)\, dE,$$

normalized to I_s, where $v_{min} = \sqrt{\frac{2e\mathcal{V}_s}{m_e}}$ when $\mathcal{V}_s > 0$ and $v_{min} = 0$ when $\mathcal{V}_s < 0$. The final expression we find is

$$\Gamma_{ph} = \left\{ \begin{matrix} 1.86\text{x}10^{10}(1.0 \text{ a.u.}) \\ 2.06\text{x}10^{11}(.3 \text{ a.u.}) \end{matrix} \right\} \cdot \left[e^{-1.6e\mathcal{V}_s(ev)} + .4e^{-.5e\mathcal{V}_s(ev)} \right]$$

for $\mathcal{V}_s > 0$ and $\Gamma_{ph} = I_s$ for $\mathcal{V}_s < 0$.

4) Secondary Electrons from Electron Impact: Secondary emission processes seem to have a threshold for occurence at about 40-50 eV incident electron energy[9]. The secondary yields rise rapidly and maximize for Al and Al_2O_3 near 300 eV[10] and at similar energies for many other materials. We have found no specific data for Cr and its oxide, and so shall use Al numbers for estimates. This means that in the quiet solar wind ($T_e \sim 20$eV) secondary emission is negligible. Under extreme conditions $T_e \sim 100$eV and secondary emission could influence the equilibrium potential. We shall present results both with and without inclusion of a secondary emission estimate.

A commonly used formula that represents reasonably well the secondary yield S(E) = number of secondaries/number of primaries is[10,11]

$$S(E) = 7.4\ S_{max}(E/E_{max})e^{-2(E/E_{max})^{\frac{1}{2}}}$$

Here E is the incident electron energy, E_{max} is the energy of maximum secondary emission ($\sim$300eV). For Al $S_{max}\sim.97$ and $S_{max}\sim2.6$ for Al_2O_3. For metallic oxides the yields can be much higher than for the pure metal ($S(E)$ can go as high as 10). For electrons with E<500eV the penetration depth is only some 10 atomic layers, so that the intrinsic oxide layers on Cr and Al might provide the higher yield factor. However the oxide layers decompose due to electron impact. Thus it is probably prudent to use the smaller pure metal yield to calculate lower limits for negative potentials.

Integration of S(E) over the electron distribution which we take to be a single Maxwellian with $T_e\sim100$eV yields the secondary current[12]

$$\Gamma_s = \sqrt{\pi}\,7.4\ S_{max}\left(\frac{kT_e}{E_{max}}\right) 5!\left[i^5\mathrm{erfc}\sqrt{\frac{kT_e}{E_{max}}}\right]e^{(kT_e/E_{max})}\ \Gamma_e(\varphi_s).$$

This expression is convenient because it says that the current of secondaries is proportional to the primary current. The quantity in brackets is

$$i^5\mathrm{erfc}(z) = \frac{2}{\sqrt{\pi}}\int_z^\infty \frac{(t-z)^5}{5!}\,e^{-t^2}dt.$$

Using Al metal numbers we find $\frac{\Gamma_s}{\Gamma_e} = .823$.

Although this factor is large it does not alter greatly the expected negative potential on the rear of an unshorted sail. This is because the correction enters logarithmically in the current balance equation.

Unshorted Sail - Shady Side. The proton density on the rear side of the sail is probably very small as discussed above. This being the case we shall consider other currents to balance with the electrons. The negative potential yielded by these computations could then be used to estimate the proton flux, and a new equilibrium computed. Neglecting the protons will give a worst case negative potential. On the shady side there is no photoemission and one must look to secondary processes to provide the currents that balance the electrons. Since the secondary current we are using is just a numerical factor times the primary current it cannot be used to balance the primary current. Equilibria between electrons and their secondaries do exist if more detailed expressions for the secondaries are used[10]. We shall instead consider the leakage current through the kapton sail film. The kapton conductivity increases with electric field, and this turns out to be an important process limiting the potential on the rear side.

To include the effect of leakage current we model the sail as a parallel plate capacitor with the front plate held at zero potential (this is close to the actual value expected). We determine the potential of the rear side by balancing the

leakage current with the net electron current. According to one model (Ref. 9, p. 3-29) the conductivity is given by

$$\sigma = \frac{\sigma_o(T)}{3}\left[2 + \cosh\left(\beta_F E^{\frac{1}{2}}/2kT\right)\right] \text{ mho/meter.}$$

E is the field in volts/meter, i.e. $E = \mathcal{V}_s(\text{volt})/2.54\times10^{-6}$ meter. Here $\sigma_o(T) \sim 10^{-16}$-$10^{-15}$ mho/meter at $T \sim 300^{\circ}K$ ($T_{sail} \sim 500$ K implies we will find an upper bound on $|\mathcal{V}_s|$); and $\beta_F/2kT \sim 7.8\times10^{-4}$. A good approximation is

$$\sigma = \frac{1}{6}\sigma_o(T)\, e^{7.8\times10^{-4}E^{\frac{1}{2}}},$$

or in c.g.s. units

$$\sigma = (1.5\times10^{-7}\text{-}1.5\times10^{-6})e^{.489\sqrt{\mathcal{V}_s}} \text{ sec}^{-1},$$

with $\mathcal{V}_s$ in volts. The current density is then

$$J_\sigma = \sigma E = (1.97\times10^{-6}\text{-}1.97\times10^{-5})\mathcal{V}_s e^{.489\sqrt{\mathcal{V}_s}} \text{ esu/cm}^2\text{-sec.}$$

This is set equal to the electron current $E\,\Gamma_e = \frac{env_e}{2\sqrt{\pi}}\, e^{\frac{e\mathcal{V}_s}{kT}}$ both with and without the correction factor for secondaries. The resultant potentials for a variety of conditions are displayed in Table 3.1.

These potentials are not particularly high compared to magnetospheric charging under substorm-eclipse conditions. The breakdown potential of the film is of the order of 1 kV, which may be sufficiently above these values. On the other hand under extreme conditions the potentials might go higher. Perhaps discharge could occur for reasons other than dielectric breakdown, such as being induced by material damage due to micrometeoroids. With these voltages a large amount of energy could be dissipated all at once in one place. The energy

1.0 a.u. Quiet Solar Wind

T_e = 20eV $\quad r_e = \frac{n}{2\sqrt{\pi}} v_e$

$n(cm^{-3})$	$\sigma_o(T)$mho/m	$\mathcal{V}_s$(volt)
10	10^{-16}	-73
10	10^{-15}	-49.5

a) No Secondaries

.3 a.u.
T_e = 100eV $\quad T_c$ = 67eV $\quad T_H$ = 431eV

n	$\sigma_o(T)$	$\mathcal{V}_s$
100	10^{-16}	-182
100	10^{-15}	-114
300	10^{-16}	-222
300	10^{-15}	-144

b) Secondaries included

.3 a.u.
T_e = 100eV $\quad T_c$ = 67eV $\quad T_H$ = 431eV

n	$\sigma_o(T)$	$\mathcal{V}_s$
100	10^{-16}	-245
100	10^{-15}	-162
300	10^{-16}	-297
300	10^{-15}	-200

c) No Secondaries

Table 3.1. Shady side potential of unshorted sail.

stored in one heliogyro blade is some 5×10^4 joules. Since shorting the front and back side together seems to present no special problems this is probably advisable.

Unshorted Sail - Sunny Side. The major currents to the front side are solar wind electrons minus secondaries, photoelectrons, and solar wind protons plus associated secondaries. It should be noted that the heliogyro will be operated in modes such that the blades will be at angles other than 90° to the spacecraft-sun line. The plasma electron current to the blade will not be a function of angle because the electrons are nearly isotropic (aside from some possible shadowing effects which are expected to be small because the gyroradius is large compared to the blade width). We shall present below, estimates of the potential as a function of angle in the context of the shorted sail.

Using the flux expressions presented above we have computed the equilibrium potentials displayed in Table 3.2. The potentials come out positive so that r_{eo} is appropriate. At .3 a.u. we have used the highest electron temperature $T_e \sim 100$eV (T_c = 6.1eV, T_H = 431eV). The results both with and without the estimate of electron secondaries are given. We note that in some cases with secondaries included the corrected electron flux is too small to balance the directed proton flux. We have indicated these cases with an asterisk (*), and have included in parenthesis revised flux and potential estimates that take into account the directed electron velocity component. In some cases this correction is sufficient to yield an

1.0 a.u. Quiet Condition

$T_e = 20eV \quad \Gamma_e = \frac{n}{2\sqrt{\pi}} \sqrt{\frac{2kT_e}{m_e}}$

$n(cm^{-3})$	V(km/sec)	$\Gamma_e(cm^{-2}sec^{-1})$	Γ_p	φ_s(volt)
10	$3x10^7$	7.5x10	$3x10^8$	+5.6
10	$8x10^7$	7.5x10 (1.22x109)	$8x10^8$	* (+5.7)

a) No Secondaries

.3 a.u. $\quad \Gamma_e = \frac{n(.177)}{2\sqrt{\pi}} \left(.9\sqrt{\frac{2kT_c}{m_c}} + .1\sqrt{\frac{2kT_H}{m_e}} \right)$

$T_e = 100eV \quad T_c = 67eV \quad T_H = 431eV$

n	V	Γ_e	Γ_p	φ_s
100	300	$2.8x10^9(3.1x10^9)$	$3x10^9$	* (+13)
100	800	$2.8x10^9(3.3x10^9)$	$8x10^9$	* (*)
300	300	$8.4x10^9(9.24x10^9)$	$9x10^9$	* (+12)
300	800	$8.4x10^9(9.9x10^9)$	$2.4x10^{10}$	* (*)

b) Secondaries included

.3 a.u.

$T_e = 100eV \quad T_c = 67eV \quad T_H = 431eV$

n	V	Γ_e	Γ_p	φ_s
100	300	$1.6x10^{10}$	$3x10^9$	+3.8
100	800	$1.6x10^{10}$	$8x10^9$	+4.7
300	300	$4.75x10^{10}$	$9x10^9$	+2.0
300	800	$4.75x10^{10}$	$2.4x10^{10}$	+2.75

c) No Secondaries

Table 3.2. Sunny side potentials of unshorted sail. Normal sunlight and proton incidence.

equilibrium. What will happen is that the secondaries which have only a few volts energy will be cut off as the potential rises. The potential cannot rise above that which will cut off the secondaries because the results with no secondaries included indicate that equilibrium is attained. It does seem remotely possible however that if the proton density were substantially higher than the electron density for a period of time (see for example Figure 3.3.) the proton flux could exceed the electron flux and give a fairly large positive voltage; the decrease of the proton flux with voltage and the increase of the effective area for electron collection are slowly varying functions of voltage.

Shorted Sail - Normal Incidence. For the shorted sail we still find all positive voltage equilibria. This means that the total plasma electron current is computed by doubling the entries for the unshorted sunny side. The results are presented in Table 3.3. Again a few cases are found where the electrons are overbalanced, and the above considerations apply.

Shorted Sail - Oblique Incidence. The heliogyro will be operated in modes where a number of blades could lie near parallel to the spacecraft-sun line, Figure 3.5. In the limit $\theta = 0$, assuming a perfectly flat blade, the photoemission goes to zero and the proton flux becomes the thermal rather than the directed flux. In this position large negative potentials can arise. In the following we construct a simplified model of the current equilibrium as a function of

1.0 a.u. Quiet Conditions

$T_e = 20eV \qquad \Gamma_e = \frac{n}{2\sqrt{\pi}}\sqrt{\frac{2kT_e}{m_e}}$

$n(cm^{-3})$	V(km/sec)	$\Gamma_e(cm^{-2}sec^{-1})$	Γ_p	φ_s(volts)
10	300	1.5×10^{9}	3×10^{8}	+3.75
10	800	1.5×10^{9}	8×10^{8}	+4.7

a) No Secondaries included

.3 a.u. $\qquad \Gamma_e = \frac{n(.177)}{2\sqrt{\pi}}\left(.9\sqrt{\frac{2kT_c}{m_e}} + .1\sqrt{\frac{2kT_H}{m_e}}\right)$

$T_e = 100eV, \quad T_c = 67eV \quad T_H = 431eV$

n	V	Γ_e	Γ_p	φ_s
100	300	5.6×10^{9}	3×10^{9}	+6.9
100	800	$5.6\times10^{9}(6.6\times10^{9})$	8×10^{9}	* (*)
300	300	1.68×10^{10}	9×10^{9}	+4.75
300	800	$1.68\times10^{10}(2.11\times10^{10})$	2.4×10^{10}	*(*)

b) Secondaries Included

.3 1.u.

$T_e = 100eV \quad T_c = 67eV \quad T_H = 431eV$

n	V	Γ_e	Γ_p	s
100	300	3.16×10^{10}	3×10^{9}	+2.45
100	800	3.16×10^{10}	8×10^{9}	+2.7
300	300	9.5×10^{10}	9×10^{9}	+1.05
300	800	9.5×10^{10}	2.4×10^{10}	+1.25

c) Secondaries not included

Table 3.3. Shorted Sail Potentials. Normal sunlight and proton incidence

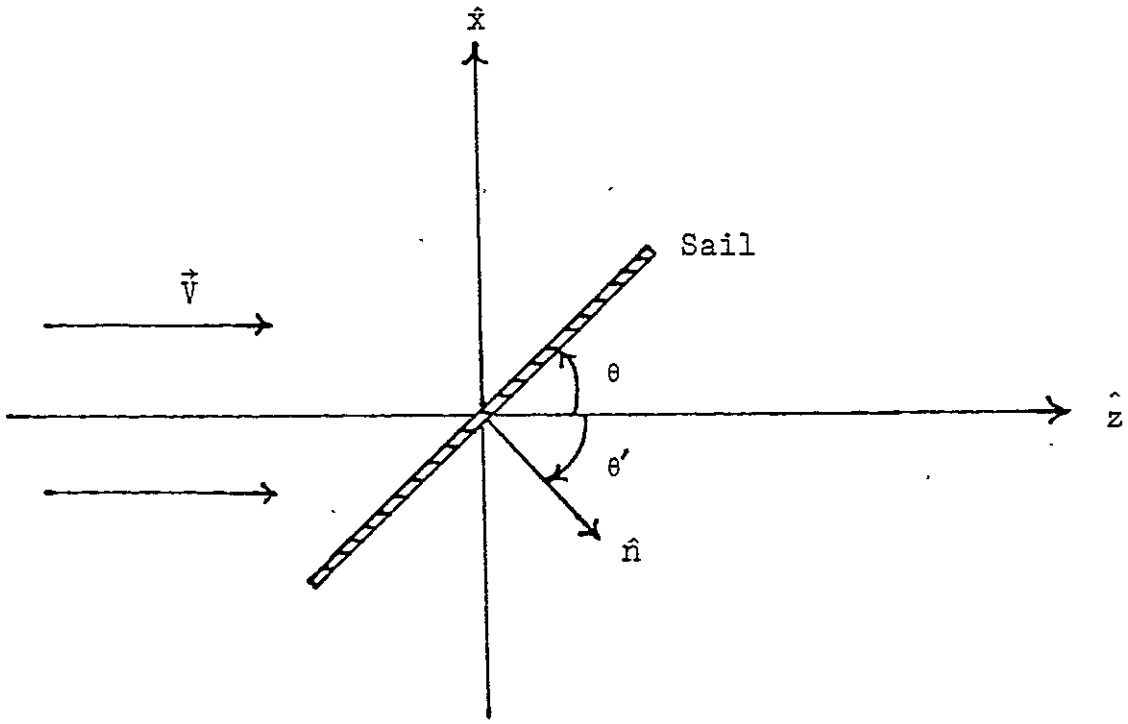

Figure 3.5. Geometry of oblique solar wind incidence.

the blade angle θ. The conclusion is that it is very unlikely that the heliogyro could ever attain large negative potentials due to angular positioning. Photoemission is always sufficient to hold the sail a few volts positive.

To construct a simple model we neglect thermal motion along the flow velocity direction ($\hat{z}$) and along the blade length ($\hat{y}$). We also neglect the fluxes to the rear of the blade. This will not significantly affect the result. The proton flux is

$$\Gamma_p = \int f_p(\vec{v})\, \vec{v}\cdot\hat{n}\, d^3v,$$

where

$$\hat{n} = \hat{z}\cos\theta' - \hat{x}\sin\theta',$$

$$\vec{v} = v_x\hat{x} + v_z\hat{z},$$

$$\vec{v}\cdot n = v_z\cos\theta' - v_x\sin\theta',$$

$$f_p(\vec{v}) = n\left(\frac{m}{2\pi kT}\right)^{\frac{1}{2}} e^{-\frac{m}{2kT}v_x^2}\,\delta(v_z - V).$$

Inserting these expressions we find

$$\Gamma_p(\theta) = n\left(\frac{m}{2\pi kT}\right)^{\frac{1}{2}} \int_{-\infty}^{V\tan\theta} dv_x (V\sin\theta - v_x\cos\theta)\, e^{-\frac{m}{2kT}v_x^2}$$

or

$$\Gamma_p(\theta) = \tfrac{1}{2}nV\sin\theta\left[1+\mathrm{erf}(M\tan\theta)\right] + \frac{n}{2\sqrt{\pi}}\cos\theta\sqrt{\frac{2kT}{m_p}}\, e^{-(M\tan\theta)^2}$$

It is easy to check that this formula has the correct limiting behavior in the limits $\theta\to 0$, $\theta\to 90^\circ$. To model the photoemission we simply use the previously calculated flux multiplied by $\sin\theta$. For an example we have taken $n = 100$, photoemission at .3 a.u., and $T_e = T_p = 80$eV. We find $\mathcal{V}_s(\theta=0) = -300$ volt,

$\mathcal{V}_s(\theta = \pi/2) = +5$ volt. $\mathcal{V}_s(\theta)$ is plotted in Figure 3.6. We see that photoemission holds the blade positive unless θ is very close to zero. The angle θ varies significantly along the blade for the real heliogyro. Thus it is unlikely that large negative potentials will ever occur. The reason for this behavior of $\mathcal{V}_s(\theta)$ is the large value of the primary photoemission flux. At $\theta = 90°$, $\mathcal{V}_s = +5$ volt, some 98% of the photoelectrons are attracted back to the sail. Thus the primary flux can be very small ($\sin\theta << 1$) and $\mathcal{V}_s$ becomes less positive. If the blade were built in electrically isolated segments a voltage differential might arise.

Proton Flux to Rear of Sail. The above calculation for $\mathcal{V}_s(\theta)$ can be adapted to estimate the proton flux to the rear of the sail. This is accomplished by letting $\hat{n} \rightarrow -\hat{n}$ and integrating over the range $V \tan\theta < v_x < \infty$. We find the expression

$$\Gamma_R(\theta) = \Gamma_o \left[-\sqrt{\pi} M \sin\theta (1 - \mathrm{erf}(M \tan\theta)) + \cos\theta e^{-(M \tan\theta)^2} \right] ,$$

$$\Gamma_o = \frac{n}{2\pi} \sqrt{\frac{2kT}{m_p}} = \Gamma_R(0) ,$$

$$\Gamma_R(90°) = 0 .$$

The ratio $\Gamma_R(\theta)/\Gamma_o$ is plotted in Figure 3.7. We see that unless the sail is lying almost parallel to the spacecraft-sun line Γ_R is a very small fraction of Γ_o (.0065 at 45°); Γ_o itself is only a fraction $1/2\sqrt{\pi}M = .043$ (M=6.5) the directed flux nV. At 45° Γ_R is a fraction 3×10^{-4} of the directed flux. It would appear that even though the metallic coating on the rear is only some 5-10% as thick as the VDA on the front the proton deposition in the kapton represented by the rearside

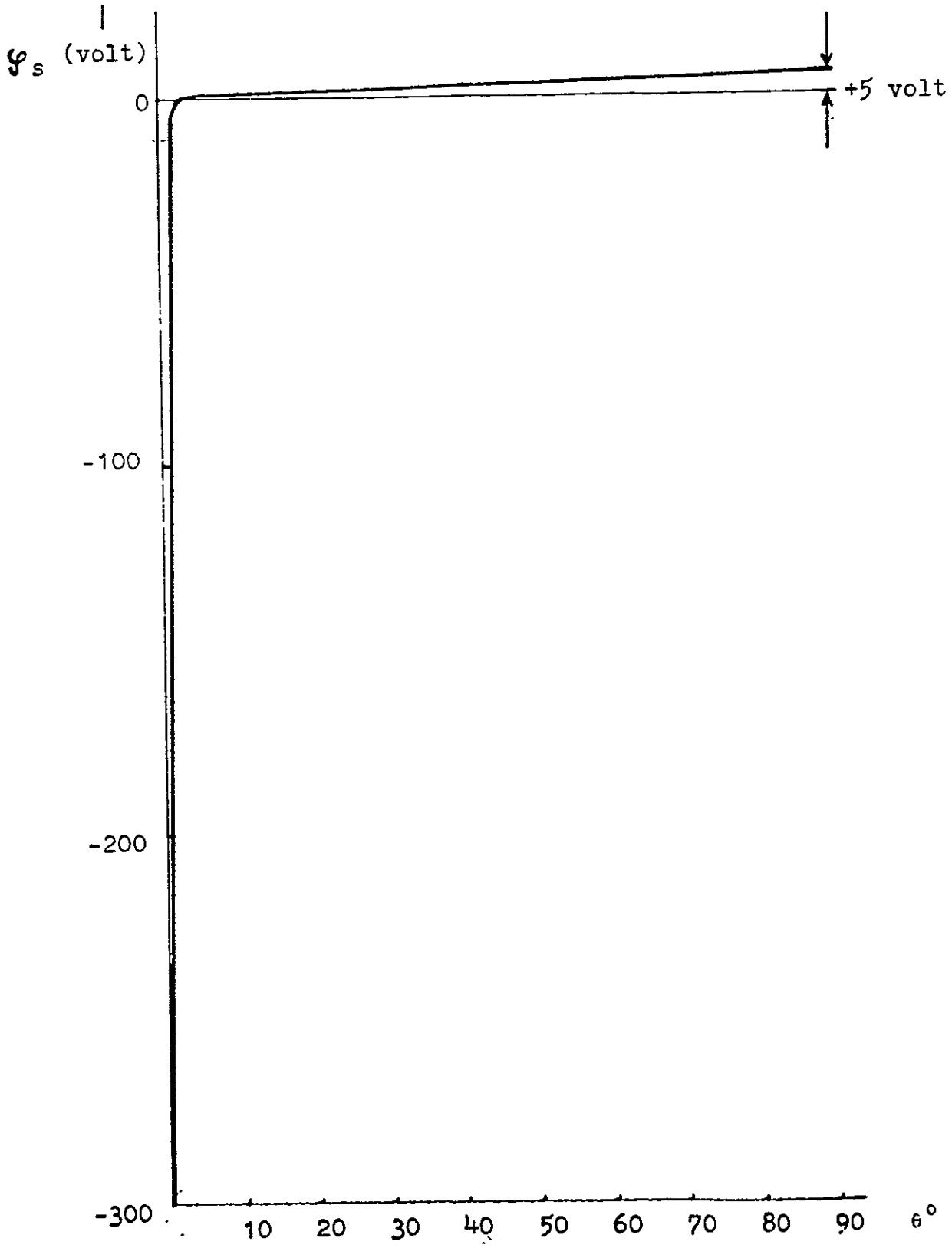

Figure 3.6. Blade potential as a function of angle.

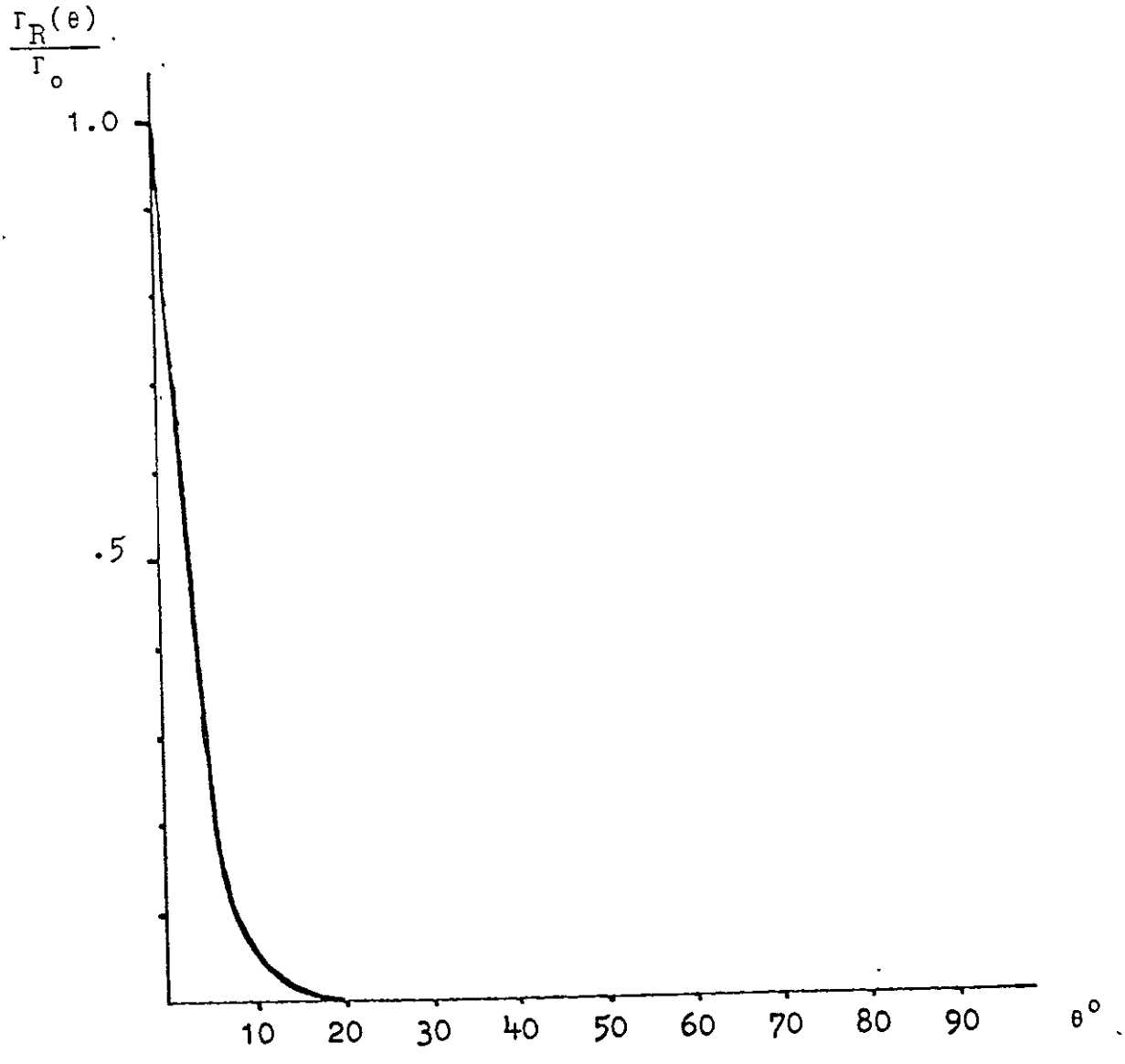

Figure 3.7. Ratio of rearside proton flux to thermal flux.

flux should be negligible compared to that coming in from the front.

4. USE OF SOLAR SAIL IN NEAR EARTH ENVIRONMENT

Several possible missions have been proposed for the sail in the vicinity of earth. Examples are (1)

a) Halley's Comet and Mars Sample and Return missions: deployment at low altitude (~800-1000 km) followed by solar radiation pressure driven orbit raising.

b) Geosynchronous orbit (GSO) operations: Use of solar sail for stationkeeping in and orbital transfer along GSO.

c) Atmospheric braking of returning interplanetary mission.

We shall discuss in the following some possible problems with earth orbit sail operations in the area of spacecraft charging and electromechanical effects within the magnetosphere. No problems which would prevent earth orbit operations have been uncovered.

A major constraint on near earth missions is the low thrust to mass ratio characteristic of the solar sail. For example in the Halley's Comet configuration only about 20% of the mass is in the payload. One finds that it would take on the order of six months to raise the orbit from 1000 km to GSO and perhaps another two months for release

from earth orbit (800 km is about the minimum altitude at which the sail could be operated, the atmospheric drag force here roughly equals the radiation pressure. At 500 km the radiation pressure is ~2% of the neutral drag and at 1000 km the neutral drag is ~10% of the solar pressure). The radiation dosages acquired during orbit raising apparently pose no threat to the kapton sail film[2]. However the extra shielding needed to protect logic circuits would lower the useful payload capacity.

In the vicinity of earth the sail will encounter various plasma and electromagnetic environments. The normal precautions that are taken to protect any spacecraft during charging events associated with magnetospheric substorms will be required for the instrument package. These include careful grounding and electrical isolation, and cautious use of dielectrics on the spacecraft surface. We shall attempt to point out in the following special problems associated with the solar sail configuration.

Most of the time the spacecraft will proceed through the very low energy plasmaspheric plasma of density $\sim 10^3/cm^3$ at low altitude to $1\text{-}10/cm^3$ at GSO and above. Due to photo-emission from the front surface aluminum and to the low energy of the plasma electrons the spacecraft will normally be held at some tens of volts positive (positive

potentials as high as 100 volts have been observed at very high altitude ~10^5 km). During eclipse the maximum negative potential will be $\varphi_s \sim -3.6\ kT_e \leq -36$ volts. Neither of these conditions are serious for spacecraft operation. During substorms this low energy plasma is swept away and replaced by energetic plasma clouds whose energy is in the range of 10 keV with density $N \sim 10/cm^3$, with associated particle fluxes.

$$\Gamma_e = 1.7 \times 10^{10}/cm^2\text{-sec}$$

$$\Gamma_p = 4 \times 10^8/cm^2\text{-sec}.$$

In the sunlight the photoelectric flux $\Gamma_{ph} = 2.6 \times 10^{10}/cm^2$-sec lowers the magnitude of the spacecraft potential substantially. With only these three fluxes taken into account and recalling that photoemission occurs only on the front side the spacecraft will charge to

$$\varphi_s = \frac{kT}{e} \ln \left[\sqrt{\frac{m_e}{m_p}} + \frac{\frac{1}{2}\Gamma_{ph}}{\Gamma_e} \right]$$

We find in the sun $\varphi_s \sim -2$kv and in the shade $\varphi_s \sim -36$kV. Backscattering and secondaries reduce these, typically by a factor of two or three. Usually the maximum charging in elipse is to approximately kTe, ie -10 kV, and in sunlight ~-.5kV. Some additional modification of these numbers will result if the finite value of the electron gyroradius is taken into account. If some dimension of the sail is small compared to the gyroradius and the plane of the sail

lies parallel to the magnetic field certain classes of particles can miss it altogether, thus lowering the electron flux and $|\varphi_s|$.

We are assuming that the front and rear of the sail are shorted together as discussed in Section 3 . It will in addition be necessary to insure that the sail and payload are also shorted together. If this were not the case they might float up to different and unpredictable potentials due to their differing material and geometric characteristics, causing problems for electronic systems connecting them.

An important concern for the solar sail is degradation of the thin Al and Cr coatings. The 1-20 kV proton fluxes in the magnetosphere are responsible for the sputtering of these metallic surfaces. One might imagine that the energy increase on attraction to a charged satellite could increase the yield. The data we have found [5] however indicates that sputtering will pose no special problem. The sputtering yield S of protons on silver holds constant at about .05 atoms/proton over proton energies ranging from 2-20 keV. We assume that 10 keV fluxes $r_p \sim 4 \times 10^8/cm^2\text{-sec}$ are present over some 25% of the six months the sail spends in earth orbit, (corresponding to substorms occuring in the midnight-dawn sector). Assuming a value $S \sim .1$ atom/proton we find the total number of sputtered atoms

$$N \sim 1.5 \times 10^{14}/cm^2.$$

The mass of aluminum removed is $\sim 7.5 \times 10^{-9}$gm giving for the layer thickness removed .3Å. This appears safely below the thickness of both the Al and the Cr. We are not certain about effects on the Al surface reflectivity. They are probably minimal because 10^{14}atoms/cm^2 represents only about one atomic layer.

Electromechanical Effects

We have also considered a number of possible electromechanical hazards that could conceivably result from operations near earth. It appears that none of these pose a threat. Most of these effects are associated with the passage into or out of eclipse. At GSO it takes some four seconds for the heliogyro to pass completely into or out of the earth's shadow. We can imagine a pair of opposing blades, one in the sun and one in the shade for a period of two minutes. We consider the following phenomena that produce mechanical forces that might be detrimental to the spacecraft.

1) Forces due to different charges on the blades: to bound possible electrostatic forces we imagine one blade in sunlight and one in shade. A voltage of 10kV on a blade implies a charge on the blade $Q \sim RV \sim (6.25 \times 10^5 cm) \times$ (33 stat volt) = 2×10^7esu. If there are two charges of this magnitude whose separation is the order of the blade length R the force between them is only 10^{-2}newtons. Thus it appears that electrostatic forces on the sail arising from spacecraft charging could not possibly compete with the blade tension 780 newton.

2) The current that could flow through the hub section during a charging-eclipse event might be on the order of

$$I = \frac{\Delta Q}{\Delta t} = \frac{2 \times 10^7 esu}{2 \text{ sec}} = 3 \times 10^{-3} amp.$$

This is much smaller than the induction current estimate of

Section 7 and thus its effects should be negligible.

Two types of non-electrostatic forces are apparent. These are 3) the torque τ arising from lack of sunlight pressure on the blade in eclipse and 4) unbalanced momentum arising from photoemission from only the sunlit blades.

3) To estimate this effect we imagine a system of two opposing blades one illuminated and one not, and assume that the moment of inertia of the system is given simply by the mass and extent of these two blades. The change in angular momentum is $\Delta L=\tau\cdot(\Delta t\sim 2\text{sec})$. The torque is provided by the radiation pressure P_s on one blade

$$\tau=P_s \int_o^R rdrw = wP_s \frac{R^2}{2} = 7.8\text{x}10^9\text{dyne-cm},$$

giving $\Delta L = 1.5\text{x}10^{10}$dyne-cm-sec. The moment of inertia of the two blades is

$$I = 2\eta \int_o^R r^2 dr = \frac{2}{3}\eta R^3$$

where $\eta\sim .4$gm/cm is the linear mass density. We find $I\approx 6.5\text{x}10^{16}$gm cm^2, and thus a rotation rate

$$\theta = \frac{\Delta L}{I} = 2.3\text{x}10^{-7}\text{rad/sec} = 1.5\text{x}10^{-5}\text{degree/sec}.$$

It appears that this torque would not be noticed. Another way to examine the effect is to calculate the Δv imparted to a single blade and compare to the orbital velocity at GSO $v\sim 3\text{x}10^5$cm/sec. We find $\Delta v = F\Delta t/m\sim .2$ cm/sec.

4) The force due to recoil of photo-electrons emitted from a blade at high potential ($\sim$10kV) works out to some $1.4\text{x}10^{-7}$dyne/cm^2, or less than 1% of the solar pressure, and

likewise its contribution to the unbalanced force.

5) Finally we consider the possibility that the electric field associated with some magnetospheric wave disturbance could disrupt the spacecraft. The type of wave we are interested in will have a period on the order of that of the flapping modes of the heliogyro blade, i.e. ~100 sec. Waves in this range are known as Pc4 waves and are observed in coherent wave trains lasting for some 10-20 cycles. The electric field strength can be as high as E~.1 volt/meter = 3.33×10^{-6} stat volt/cm.

For a simple model we imagine again a single blade charged up to 10kV, so that the charge estimate of 1) implies a charge density $\sigma \sim 4 \times 10^{-2}$ esu/cm^2. This charge density and field imply a force on the blade

$$\sigma E \sim 1.2 \times 10^{-7} \text{ dyne/cm}^3 << P_s,$$

and thus the whole spacecraft is not moved significantly. We next examine what might happen when this small force is applied in resonance with a blade normal mode. We shall calculate with a mathematically very simple model. We imagine a blade tied at both ends under tension T=385 newton = 3.85×10^7dyne (or about half the blade tension), the average tension along the actual blade. We also neglect damping (which is small: Q~1000[6]) and assume E is normal to the blade and in perfect resonance with its lowest mode. The

wave equation for the blade displacement is

$$\eta \frac{\partial^2 u}{\partial t^2} - T \frac{\partial^2 u}{\partial x^2} = F_{ext} ,$$

The lowest mode of the unperturbed blade is

$$u = \sin \frac{\pi x}{R} \cdot \mathrm{Sin}\ \omega_1 t$$

with $\omega_1 = \frac{\pi}{R}\sqrt{\frac{T}{\eta}} = c \frac{\pi}{R} = 4.9 \times 10^{-2} \mathrm{rad/sec}$

(this gives a period of 127 sec). We also assume for mathematical simplicity that the external force has the constant shape $\sin \frac{\pi x}{R}$ over the blade. In fact the E field wave lengths we are considering are much longer than the blade and the force is effectively constant in space and sinusoidal in time. We are then considering the coupling of this force to the lowest blade mode. The wave equation is thus

$$\frac{\partial^2 u}{\partial t^2} - c^2 \frac{\partial^2 u}{\partial x^2} = \beta \sin \frac{\pi x}{R} \sin \omega_1 t.$$

The constant β is given by the force per unit length divided by the mass per unit length.

$$\beta = \frac{F}{\eta} = \frac{\sigma w E}{\eta} = 2.66 \times 10^{-4} \frac{cm}{sec^2}.$$

Assuming the displacement is zero at time zero we find

$$u(t) = \frac{\beta}{2\omega_1^2} \sin \frac{\pi x}{R} (\sin \omega_1 t - \omega_1 t \cos \omega_1 t),$$

and the amplitude grows linearly,

$$A(t) \sim \frac{\beta t}{2\omega_1} .$$

After twenty cycles or 2,540 sec $\Delta \sim 7.0$ cm. This appears safely small. In particular it should be recalled that to compute the force we have used an estimate for the charge density that is rather extreme, and also we neglected damping. In any case if the heliogyro were developed for use within the magnetosphere it would be prudent to calculate more realistically the interaction with probable magnetospheric wave modes, using a correct heliogyro blade model.

In summary we have found no special problems of a plasma or electromechanical nature that would prevent the use of the solar sail near earth.

5. DEPLOYMENT PROBLEMS DUE TO STATIC ELECTRICITY

It is important to know whether charge residing on solar sail material in the rolled up configuration will present an obstacle to its unrolling. The major feature of the solar sail that seems to minimize such problems is the fact that it is coated on both sides with conductors and the two coatings are shorted together. Separated static charge can reside only on good insulators. It seems likely that with careful handling the only surface insulator present will be the oxide films that inevitably develop on fresh vapor deposited metal surfaces. These are typically very thin (30-100Å) and will not sustain a high voltage. The resistivity of the film is a few orders of magnitude less than that of the bulk material and breakdown potentials are of the order of a few volts. It thus appears that we will be seeking and attempting to quantify rather small effects. This is borne out by the observation that static electricity apparently ceases to be a problem after the metal film is deposited. [1] In the following we shall consider a model of electrostatic forces that should exist even between metallized layers, due to the contact potential between dissimilar metals, and compare the forces derived to that applied in unrolling the sail in the helio-gyro configuration. The same consideration should apply to the square sail geometry for the case where storage is accomplished by rolling.

MINIMUM DEPLOYMENT FORCE

The unfurling of the helio-gyro is accomplished by spinning the vehicle with thrusters to provide sufficient centrifugal force to unroll the blades to a length of ~150 meters. At this point the blades are given a pitch and solar radiation pressure provides the rotation force and the blades are slowly released. The final length is R_{max}~6,250 meter = 6.25 x 10^5cm. The rotation angular frequency Ω during deployment is such that the product $R\Omega^2$ = constant $\equiv \beta^{2(2)}$. Since the rotation period at maximum extension is 200 sec. we establish that $\beta^2 = 6.6 \times 10^2 cm/sec^2$. The maximum blade tension is specified to be F_{max}~760 newton. We are interested in the minimum force in order to establish that it is sufficient to overcome any drag due to static electricity. The centrifugal force due to the blade deployed to radius R is

$$F = \int_o^R dm \frac{v^2}{\pi} = \eta \int_o^R dr \frac{r^2\Omega^2(R)}{\pi} = \Omega^2(R)\eta \frac{R^2}{2} ,$$

where η is the linear mass density. Thus F scales linearly with R and we find F_{min}~20 newton.

STATIC FORCE MODEL

Figure 5.1 illustrates the geometry in the rolled up configuration. Opposite charges on the opposing surfaces will attract, and retard the unrolling. Free charge could

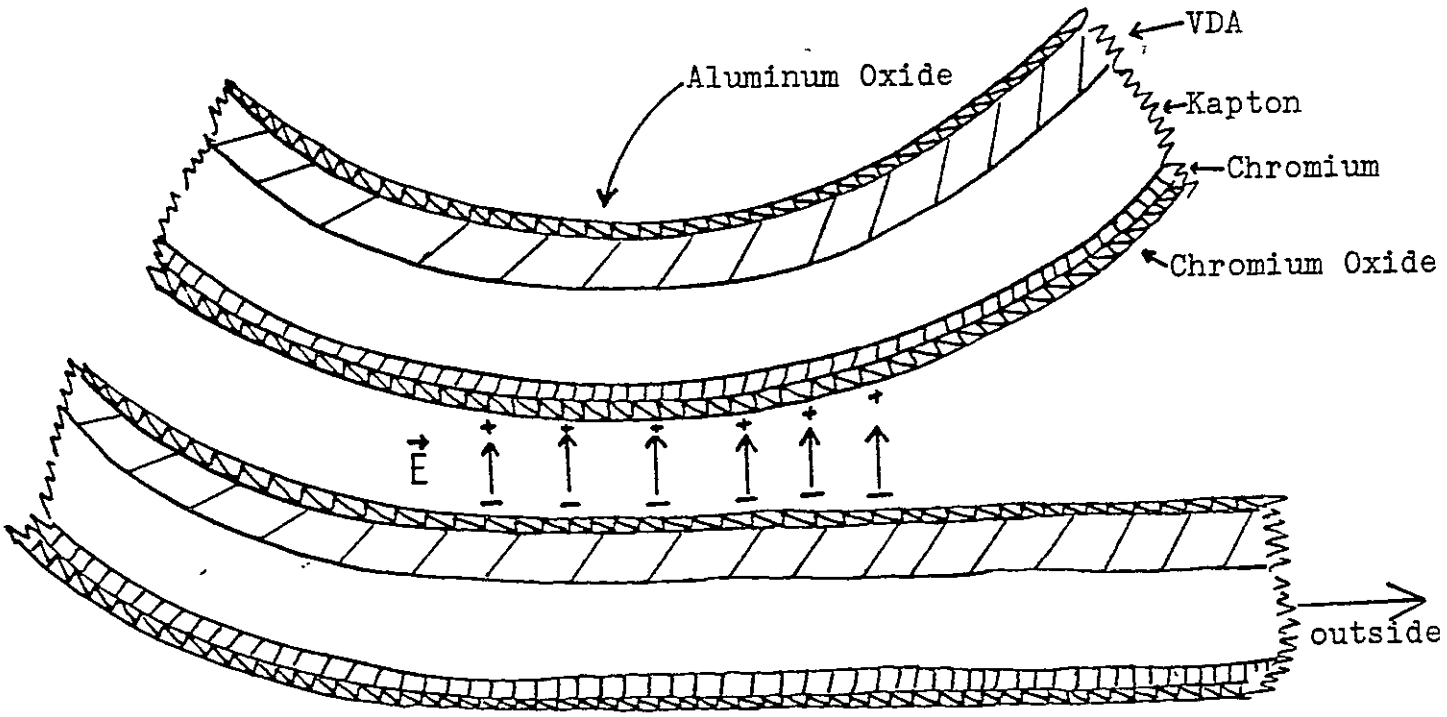

Figure 5.1. Rolled up geometry.

have been deposited on the metallic oxide layers during production and stowage. We feel that this would have dissipated due to leakage conduction by the time of deployment. Using values [3], Table 5.1 for the bulk Al_2O_3 conductivity, which are typically much larger than that of the thin film[4] we find that the characteristic time for dissipation of static charge $\tau_c = \frac{\varepsilon}{4\pi\sigma}$, ($\varepsilon \sim 10$), are sufficiently small, even at room temperature.

T(^{o}K)	ρ(Ωcm)	σ(sec^{-1})	τ_c(sec)
287	10^{16}	9×10^{-5}	8.8×10^{3}
573	3×10^{13}	3×10^{-2}	26.5
1073	3.5×10^{14}	2.6×10^{3}	3.1×10^{-4}

Table 5.1 - Bulk conductivity and charge dissipation time for Al_2O_3.

If there is a potential difference between the Cr and Al surfaces, however, static charge will remain. Such a potential difference might arise due to the contact potential V_c between Cr and Al, which is equal to the difference between their work functions and the order of 1.0 volt. This establishes the amount of charge that remains on the facing surfaces, and determines the force between layers. Contact is established by sail shorting and/or surface pressure contact. This effect is well known[5,6] as a mechanism for transferring static charge between dissimilar conductors. The geometry is essentially that of a parallel

plate capacitor, Figure 5.2. The electric field is $E=V_c/d$, surface charge $\sigma = E/4\pi = V_c/4\pi d$, and force per unit area $F=\sigma E = V_c^2/4\pi d^2$. Appropriate values of d are discussed below.

The force retarding unrolling will be taken to be the average energy per unit length required to separate the layers. The metal surfaces come into close contact only over a very small fraction of the total area, and, since the film is flexible, areas in close contact can be separated by a peeling motion; whereas separating them in the perpendicular direction would require much more applied force. We estimate the forces according to two models. In the first we assume that the surface static charge is free to flow as the surfaces are separated. In this case the force per unit length when the separation is x is $F(x) = V_c^2/4\pi x^2$ and the average force is

$$F_c = w\int_d^\infty \frac{V_c^2}{4\pi}\,\frac{dx}{x^2} = w\,\frac{V_c^2}{4\pi d} \quad ,$$

where w = 800 cm is the width of the blade. We have calculated this as the energy necessary to separate capacitor plates held at constant potential V_c to infinity. This is correct for the unrolling problem as well because the energy required is independent of the mode of separation. The second model we use assumes that the original amount of charge remains on the surfaces as they are separated. In this case the force is much larger. Which case applies will

$$E = \frac{V_c}{d}$$

$$\sigma = E/4\pi$$

$$F = \sigma E = \frac{V_c^2}{4\pi d^2}$$

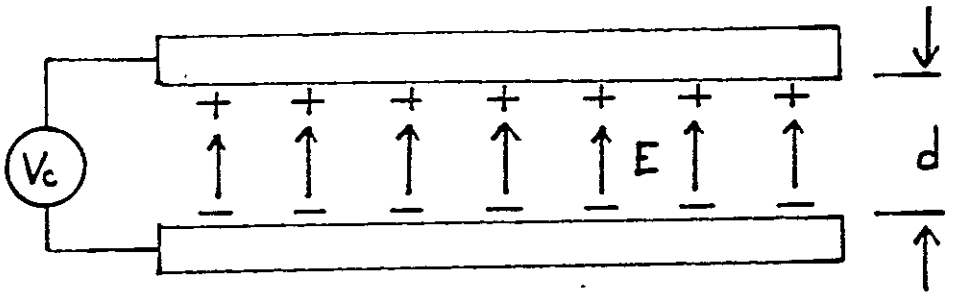

Figure 5.2. Parallel plate geometry.

depend on the rate of separation, that is on the characteristic time for separation compared to τ_c, the characteristic time for charge dissipation. For this second model we have only a crude estimate of the force. The model is illustrated in Figure 5.3. We simply estimate the energy it takes to take the charge from $\theta=0$ to $\theta_{max}=\pi/2$ above an infinite plane of charge, and divide by $(\pi/2)R_\bullet$. We shall argue later that this model grossly overestimates the energy and that a much smaller value of θ_{max} is appropriate. The force one ends up with is $F_x=wR_\bullet V_c^2/4\pi d^2$, much larger than F_c.

To complete the force estimates requires estimates of d; for the helio-gyro $R_\bullet$=30cm. We consider, starting with the smallest, the characteristic spacings involved. The VDA (vapor deposited aluminum) thickness is $d_v=10^{-5}$cm, with uncertainty $d_{sv}=10^{-6}$cm. We shall disregard the Cr layer. The Kapton thickness is $d_k=2.5\times10^{-4}$cm with uncertainty $d_{sk}=5\times10^{-5}(-20\%)$. The final dimension we wish to consider is what we shall call the "loose wrap", separation $d_{\ell w}=2.5\times10^{-3}$cm(1), a rough estimate of the spacing when the sail is rolled up before deployment. However due to the presence of battens lying across the sail some 10-30% of the area will be pressed together. Thus the force for $d=d_{sk}$ will probably give the most useful comparison with F_{min}.

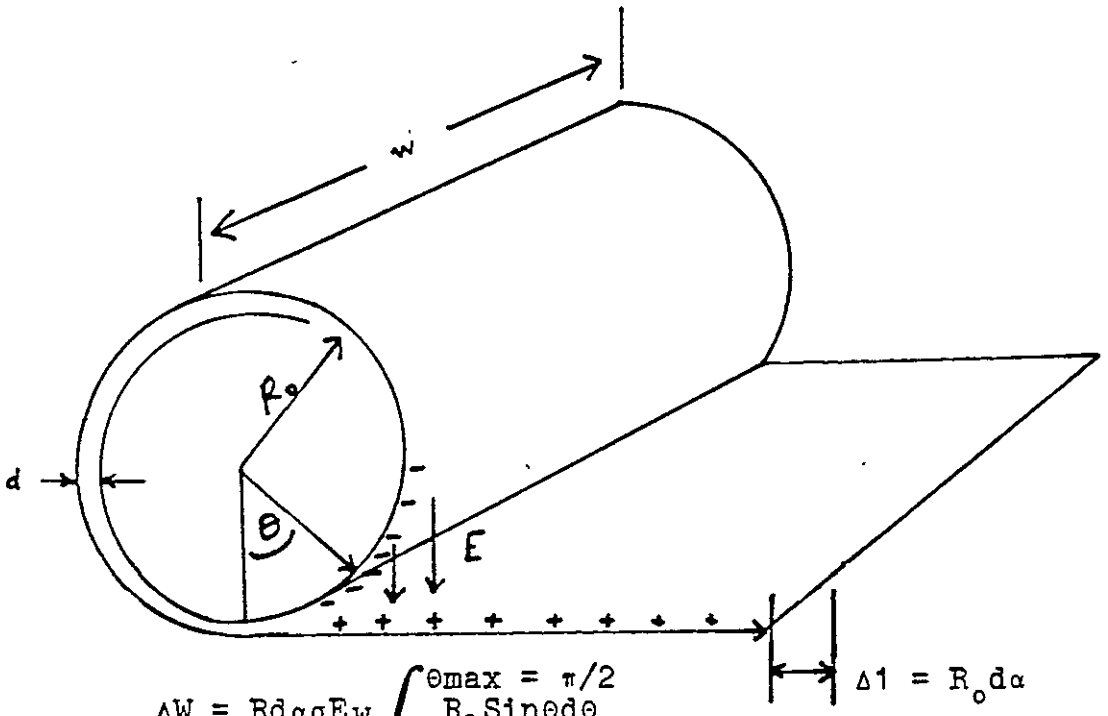

$$\Delta W = R d\alpha \sigma E w \int_0^{\theta max = \pi/2} R_o \sin\theta d\theta$$

$$E = \frac{V_c}{d} \qquad \sigma = \frac{V_c}{4\pi d}$$

$$F_s = \frac{\Delta W}{\Delta 1} = \frac{w R_o V_c^2}{4\pi d^2}$$

Figure 5.3. Geometry for force at constant charge.

The distances and forces are displayed in Table 5.2.

d_i(cm)	F_c(nt)	F_s(nt)
$d_{sv}=10^{-6}$	7.07×10^{-3}	2.12×10^{5}
$d_v=10^{-5}$	7.07×10^{-4}	2.12×10^{3}
$d_{sk}=5\times10^{-5}$	1.4×10^{-4}	85
$d_k=2.5\times10^{-4}$	2.8×10^{-5}	3.4
$d_{ew}=2.5\times10^{-3}$	2.8×10^{-6}	3.4×10^{-2}

Table 5.2. Electrostatic Forces Retarding Unrolling of Sail.

We see that if F_c is applicable no problems will arise. However, if F_s is involved the forces are larger. We do not feel that F_s will apply for the following reasons. In the first place raising a charge a distance R implies a 6000 volt potential difference. However since the thin oxide coatings will only sustain a few volts before breaking down(7), they will only separate to a few times d before breaking down and thus the force should be of the order of a few times F_c. Aside from this the enhanced conductivity for thin oxide films, which is described in the literature as being something like a few orders of magnitude [4] should be sufficient to insure that the charge equilibration time is short compared to the time of about 60 seconds it takes the sail drum to rotate through $\pi/2$ radians. Values of σ inferred from the literature (eg. $R\sim10^3$-10^5-$10^7\Omega$ for an oxide layer of order 10^{-6}cm thick and .01cm^2 in area, (Ref.8) give

$\tau_c \sim 10^{-5}$-10^{-3}-10^{-1}sec)) indicate that this is the case. Thus without further detailed information we tend to think that the forces F_c are applicable, and static charge should be no problem. We should emphasize however that thin film conductivity values vary widely with temperature and method of preparation.

In summary we feel that there is no strong indication of problems of deployment due to static electricity. However we have based our analysis on the average forces involved. We have only crudely analyzed the possibility that small localized areas that are in very close contact might stick together, and the possibility the pliability of the Kapton would allow the average separation to decrease.

6. ELECTROMECHANICAL OSCILLATIONS OF THE SOLAR SAIL

The goal addressed in this section is to answer the question "Does the interaction with the solar wind plasma cause the sail to develop unstable modes of oscillation?" In sailing parlance "Does the sail luff?" This question is deceptive in its simplicity hiding a myriad of possible mechanisms. To illustrate, consider the equation of motion for a membrane

$$\rho \frac{\partial^2 y}{\partial t^2} - T \nabla^2 y = f$$

where for the case at hand

$$f = \sigma E_x + P + S$$

$$= \begin{matrix}\text{electrostatic} \\ \text{pressure}\end{matrix} + \begin{matrix}\text{plasma} \\ \text{pressure}\end{matrix} + \begin{matrix}\text{photon} \\ \text{pressure}\end{matrix}$$

We are interested in perturbations from equilibrium caused by the first two terms. As a worst case we shall neglect the photon pressure which would appear to be universally stabilizing. Our treatment consists of examining a few cases which are amenable to calculation then making an informed guess as to the magnitude of the problem. This section, while only a few pages long, required almost as much research effort as the rest of the report. There is almost no directly relevant literature and so much of the work must be original. There remain numerous loose ends and the final answer is far from definitive. Nonetheless, with these substantial qualifications, we find that the answer to the question at hand is "Probably not."

Gas Dynamic Coupling

We first illustrate the problem by considering the coupling of oscillations on the surface of the solar sail to sound waves in the surrounding gas. This ease is amenable to calculation and demonstrates one important dimensionless parameter associated with electromechanical oscillations. The result of the calculation is quite clear. This mechanism cannot cause luffing.

The problem is illustrated by analogy. Consider a cylinder, of infinite length, which has a thin membrane (a drum head) stretched across it as shown in Figure 6.1. Morse and Ingard [1] have considered the similar problem of a vibrating string coupled to sound waves in a gas. Review of their work indicates the complicated nature of these problems. In this section we demonstrate some of the salient features of such a system. A simple model is used which substantially reduces the algebraic complexity of the problem. The solutions presented here are more easily understood than those in Morse and Ingard and exhibit substantially the same physics.

If the drum head is struck with a hammer it will oscillate with a characteristic frequency determined by the parameters of the system. The oscillation of the drum head will set up sound waves in the cylinder. These sound waves will propagate down the cylinder away from the drumhead.

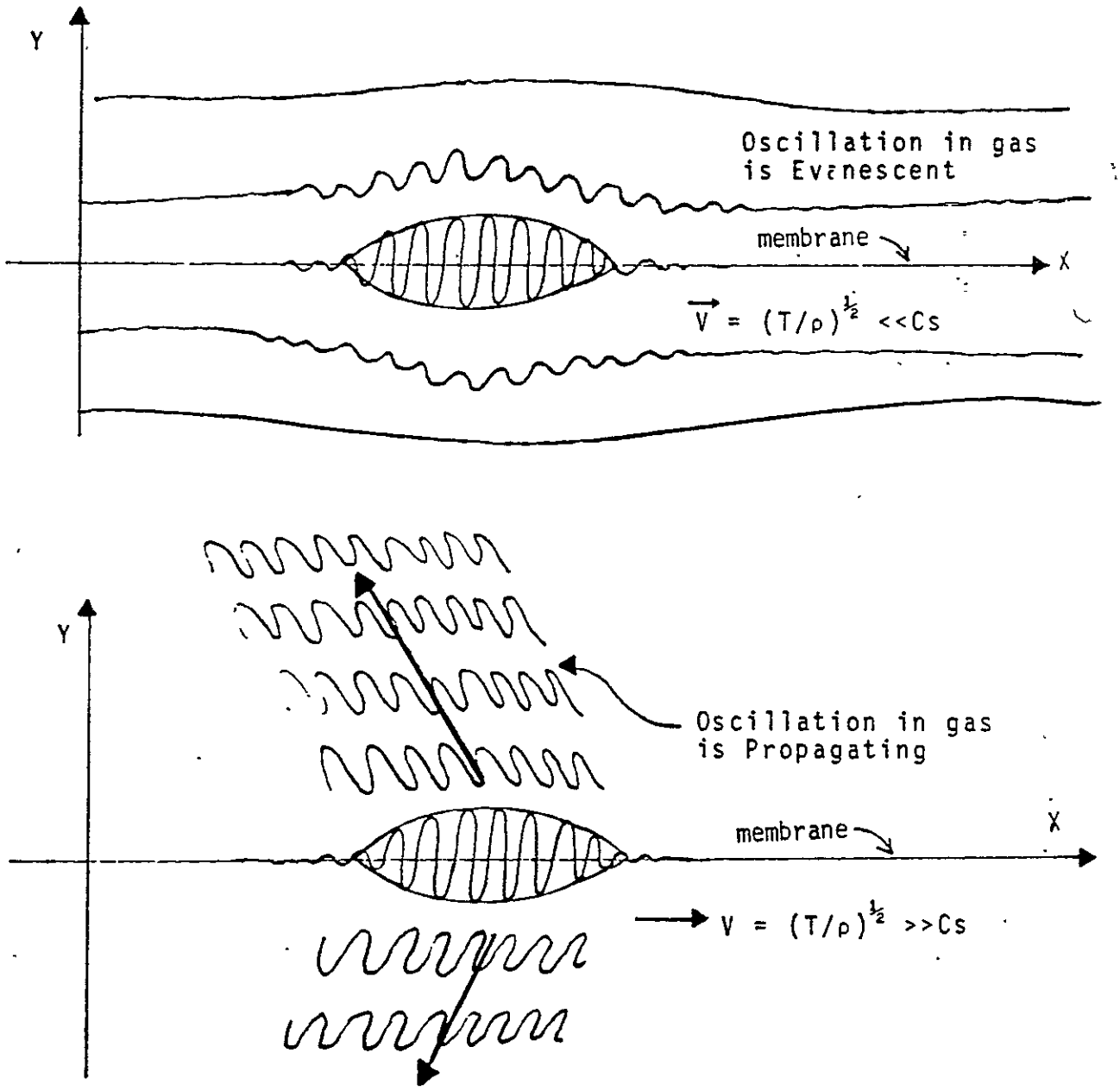

Figure 6.1. Waves propagating on a membrane coupled to a surrounding gas. When the wave speed on the membrane $V = (T/\rho)^{\frac{1}{2}} << C_s$, the sound speed in the gas, then the mass of the gas loads the string. When $V >> C_s$ sound waves are radiated from the string in a process analogous to Cherenkov radiation.

Consider for the moment the modes of oscillation with dimensions small compared to that of the cylinder i.e. wavelengths $\lambda << R$. In this limit one may neglect the details of the boundary conditions and treat the membrane as an infinite sheet embedded in an unbounded medium. What are the modes of oscillation of this system?

Waves propagate on an infinite membrane with the characteristic dispersion relation

$$\omega = \left(\frac{T}{\rho}\right)^{\frac{1}{2}} K$$

where $\omega = 2\pi f$ is the characteristic frequency

$K = 2\pi/\lambda$ is the wave number for λ the wavelength

T is the tension in the membrane

ρ is the density of the membrane.

The characteristic dispersion relation for sound waves in a gas is

$$\omega = C_s K$$

where C_s is the sound speed which depends upon the temperature and molecular composition of the gas.

This is not a complete description of the problem at hand. The presence of the gas around the membrane causes additional forces to act upon the membrane thus modifying its characteristic dispersion. Similarly the dispersion relationship for waves propagating in the gas is modified by forces exerted by the membrane upon the gas. The oscillations of the membrane and the gas are thus coupled.

Two limits suggest themselves. Whenever the wave speed on the membrane is less than the sound speed in the gas, i.e. $(T/\rho)^{\frac{1}{2}} << C_s$ the gas can respond essentially instantaneously to deformations of the membrane. Thus an oscillation propagating slowly across the membrane will simply push the gas back and forth. In the alternative limit $(T/\rho)^{\frac{1}{2}} >> C_s$ the gas cannot respond instantaneously to the oscillations of the membrane. In this limit an oscillation propagating across the membrane will excite waves in the gas which propagate away from the membrane. The two regimes are illustrated in Figure 6.1. These effects will now be illustrated by detailed calculation.

The membrane is described by the linearized wave equation

$$\rho \frac{\partial^2 \eta}{\partial t^2} - T \frac{\partial^2 \eta}{\partial x^2} = p- - p+$$

where η is the displacement of the membrane in the y direction

and $p\pm$ are the pressures exerted by the gas for $y \gtrless 0$.

The gas is described by equations for the conservation of number density n and momentum, and an equation of state relating the pressure $p\pm$ to the number density. These are

$$\frac{\partial n}{\partial t} + n_o \frac{\partial V_x}{\partial x} + n_o \frac{\partial V_y}{\partial y} = 0$$

$$n_o m \frac{\partial V_x}{\partial t} = - \frac{\partial p}{\partial x} \qquad n_o m \frac{\partial V_y}{\partial t} = - \frac{\partial p}{\partial y}$$

$$p = \left(\frac{\gamma p_o}{n_o}\right) n$$

where m is the mean molecular weight

$\gamma = 1$ for isothermal expansion

$\gamma = 3$ for adiabatic expansion

Combining the gas equations one finds

$$\frac{\partial^2 p}{\partial t^2} - C_s^2 \left(\frac{\partial^2 p}{\partial x^2} + \frac{\partial^2 p}{\partial y^2}\right) = 0$$

which describes the propagation of sound waves in the gas characterised by a sound speed $C_s = (\gamma p_o / n_o m)^{\frac{1}{2}} = (\gamma T_o / m)^{\frac{1}{2}}$ where T is the temperature.

The gas and membrane are further coupled by the requirement that the component of gas velocity in the y direction match the velocity of the Y displacement of the membrane.

Thus $V_y = \frac{\partial n}{\partial t}$ on the membrane. Using the momentum equation we relate this to the pressure and find

$$\frac{\partial^2 n}{\partial t^2} = - \frac{1}{n_o m} \frac{\partial p}{\partial y}$$

which for linear perturbations of the membrane is to be evaluated on equilibrium surface y = 0.

In the limit $(T/\rho)^{\frac{1}{2}} < C_s$ the waves do not propagate into the gas and the solutions for the pressure may be represented as

$$p = \begin{cases} \hat{p} e^{-\alpha y} & y > 0 \\ \hat{p} e^{\alpha y} & y < 0 \end{cases}$$

where α is a constant to be determined from the gas propagation equation

Combining these equations one finds

$$p\pm = \pm\left(\frac{n_o m}{\alpha}\right) \frac{\partial^2 \eta}{\partial t^2} \Rightarrow p- - p+ = -\left(\frac{2n_o m}{\alpha}\right) \frac{\partial^2 \eta}{\partial t^2}$$

Thus we find that the equation describing the coupled oscillations is:

$$\left[\rho + \frac{2n_o m}{\alpha}\right] \frac{\partial^2 \eta}{\partial t^2} - T \frac{\partial^2 \eta}{\partial x^2} = 0$$

This equation admits to a very simple interpretation. The membrane mass density per unit area ρ is replaced by an effective mass density per unit area $\rho^* = \rho + (2n_o m/\alpha)$. So we see that the mass of gas contained in the perturbed pressure sheath of thickness $L = 1/\alpha$ simply loads the membrane.

Now let us examine this limit in slightly more detail by considering a specific perturbation of the form

$$\eta = \hat{\eta} \sin(kx-\omega t)$$

$$p = \begin{cases} \hat{p} e^{-\alpha y} \sin(kx-\omega t) & y>0 \\ \hat{p} e^{\alpha y} \sin(kx-\omega t) & y<0 \end{cases}$$

The dispersion relation becomes

$$\left(\rho + \frac{2n_o m}{\alpha}\right) \omega^2 - T K^2 = 0$$

where

$$\alpha = K\sqrt{1-\left(\frac{\omega}{KC_s}\right)^2}$$

This dispersion relation is cubic in ω^2 thus exhibiting three double modes corresponding to the modified sound waves on either side of the membrane, and the basic membrane mode.

Now in the limit $(T/\rho)^{\frac{1}{2}} >> C_s$ one takes as the pressure perturbation a representation yielding outgoing waves.

$$p = \begin{cases} pe^{i(Ky+Kx-\omega t)} & y>0 \\ pe^{i(-Ky+Kx-\omega t)} & y<0 \end{cases}$$

From which we obtain the dispersion relation

$$\left(\rho + i\,\frac{2n_o m}{\alpha}\right)\omega^2 - T\,K^2 = 0$$

where

$$\alpha = \frac{\omega}{C_s}\sqrt{1-\left(\frac{KC_s}{\omega}\right)^2}$$

Now one finds solutions for the membrane mode of the form

$$\omega = \omega_r + i\gamma$$

where

$$\omega_r = \left(\frac{T}{\rho}\right)^{\frac{1}{2}} K$$

$$\gamma = -\left(\frac{n_o m C_s}{\rho}\right) \Rightarrow \text{ dampening.}$$

Thus the membrane modes are damped by energy radiated into sound waves.

Now let us examine the effect of a gas flowing across the membrane. While a number of additional complications could be introduced, we shall only examine the effect of doppler shift which causes the frequency associated with the moving medium to be transformed from ω to $\omega - \underset{\sim}{K}_o \cdot \underset{\sim}{V}_o$. Thus pressure perturbations associated with a gas moving with velocity $v = v_o \underset{\sim}{e}_x$ will obey the equation

$$\left[(\omega - K V_o)^2 - K^2 C_s^2\right] p + C_s^2 \frac{\partial^2 \rho}{\partial y^2} = 0$$

which has evanescent solutions

$$p = \begin{cases} \hat{p}_e - \alpha y_e i(Kx-\omega t) & y>0 \\ \hat{p}_e \alpha y_e i(Kx-\omega t) & y<0 \end{cases}$$

whenever

$$\alpha^2 = K^2 \left[1 - \left(\frac{\omega}{KC_s} - \frac{V_o}{C_s}\right)^2\right] > 0$$

Now consider the case $\frac{\omega}{K} << V_o \lesssim C_s$. The appropriate solutions are the evanescent ones since $\alpha^2 > 0$. The boundary condition is unmodified but the momentum equation is doppler shifted. One obtains

$$\hat{\eta} = \frac{1}{\omega}\left(\frac{1}{\omega - KV_o}\right)\frac{1}{n_o m}\frac{\partial p}{\partial y}$$

and hence

$$\hat{p}- - \hat{p}+ = \omega(\omega - KV_o)\left(\frac{2n_o m}{\alpha}\right)\hat{\eta}$$
$$\simeq -\omega^2\left(\frac{KV_o}{\omega}\right)\left(\frac{2n_o m}{\alpha}\right)\hat{\eta}$$

So there results the dispersion relation

$$\left[\rho - \left(\frac{KV_o}{\omega}\right)\left(\frac{2n_o m}{\alpha}\right)\right]\omega^2 - T K^2 = 0$$

Note now that the effective mass $\rho^* = \rho - (KV_o/\omega)(2n_o m/\alpha)$ may become negative in which case an instability would develop. The physical mechanism is as follows. The mass displaced by the sail is convected along by the flow thus shifting by 180 degrees the phase with which the mass loading is applied to

the membrane. The resulting instability grows by extracting free energy from the flow.

A basic dimensionless parameter $\epsilon = (n_o mL/\rho)$, where $L = \alpha^{-1}$ is a typical length, characterizes the gas dynamic coupling. This parameter simply measures the effective mass loading which the gas applies to the membrane.

For the solar wind $n_o m \lesssim 1.6\times10^{-16} gm/m^3$. For the sail $\rho \simeq 3$ gm/m^2 thus $\epsilon = 1$ requires $L = (\rho/n_o m) \gtrsim 2\times10^{16}$ meters. This astronomically large number indicates that gas dynamic mass coupling is not significant, since L is many orders of magnitude greater than a typical sail dimension. Alternatively note that in the streaming case $L \simeq (V_o/\omega)$ where $V_o = 800$ Km/sec and $\omega \simeq 5\times10^{-2}$ rad/sec are typical for the solar wind and the sail respectively. Thus $L = 1.6\times10^{7}$ meters and hence $\epsilon \simeq 10^{-11}$ so we are many orders of magnitude away from instability.

Thus we can say with certainty that the solar wind is of such low mass density that it cannot couple significantly to the sail through these mechanisms.

Resonant Forcing

Obviously we must look elsewhere for potential sources of instability. Treating the solar wind as a simple gas rather than as a plasma neglects the important electrostatic couplings between the solar sail and solar wind. To better understand these couplings we now examine the case of resonant electrostatic forcing of the sail. These are forced oscillations caused by those fluctuations of the solar wind which are of such a frequency as to resonate with the natural frequency of oscillation of the sail.

Consider a membrane subject to external forces. The equation describing linear oscillations of such a membrane is:

$$\rho \frac{\partial^2 \eta}{\partial t^2} - T \frac{\partial^2 \eta}{\partial x^2} = \Delta F$$

where ΔF is the perturbing force exerted on the surface of the membrane. In the previous section we examined perturbing forces caused by a pressure differential across the membrane. Now we examine electrostatic perturbing forces given by

$$\begin{aligned} \Delta F &= \sigma_o \Delta E_y + \Delta \sigma E_{yo} \\ &= \Delta \frac{E_y^2}{4\pi} \\ &= \Delta U_\varepsilon \end{aligned}$$

where $U_\varepsilon = (E_y^2/4\pi)$ is the electrostatic energy density evaluated at the membrane surface.

In equilibrium, as has been discussed in earlier parts of this report, a plasma sheath approximately one Debye length

thick will form about the sail. A typical particle will transit this sheath in times $\tau \sim \omega_p^{-1}$, which for ions is typically a few microseconds. The natural frequencies of oscillation of the solar sail are many orders of magnitude less than this thus the sheath responds quasi-statically to fluctuations in the solar wind. Therefore we take

$$\Delta U_\varepsilon = U_\varepsilon(\Delta\alpha/\alpha)$$

where $U_\varepsilon \sim \frac{1}{2} n m_i U_o^2 \sim 10^{-7}$ erg/cm^3, which is the wind streaming energy density, and $(\Delta\alpha/\alpha)$ is the relative amplitude of a fluctuation in the solar wind.

Typical unforced oscillations of the membrane are of the form

$$\hat{\eta} = \hat{\eta} \sin(\pi x/L)\sin\omega_1 t$$

where $\omega_1 = (\pi/L)(T/\rho)^{\frac{1}{2}}$

Now if we consider a resonant fluctuation for which

$$\frac{\Delta\alpha}{\alpha}(x,t) = \frac{\Delta\alpha}{\alpha} \sin(\pi x/L) \sin\omega_1 t$$

then the sail will respond with a secularly growing oscillation. For an initial displacement of zero, one finds the solution

$$\eta = \frac{1}{2\omega_1^2}\left(\frac{U_\varepsilon}{\rho}\right)\left(\frac{\Delta\alpha}{\alpha}\right) \sin(\pi x/L)(\sin\omega_1 t - \omega_1 t \cos\omega_1 t)$$

And thus the amplitude of the secular growing term is

$$\eta \sim \frac{1}{2}\left(\frac{U_\varepsilon}{\rho}\right)\left(\frac{\Delta\alpha}{\alpha}\right)\left(\frac{t}{\omega_1}\right)$$

Now numbers

$$U_\varepsilon = 10^{-7}\text{ergs/cm}^3 = 10^{-8}\text{joules/m}^3$$

$\rho = 3\times10^{-3}\,\mathrm{Kg/m^2}$

$\omega_1 = 4.9\times10^{-2}$ rad/sec

which result in an amplitude

$$\eta \sim .06 \left(\frac{\Delta\alpha}{\alpha}\right) \quad (\omega_1 t)\ \text{cm}$$

Thus $(\Delta\alpha/\alpha) \sim 0.5$, indicating a fifty percent change in amplitude of the solar wind, would require $\omega_1 t \sim 33$, i.e. 33 cycles, in order to produce a wave with amplitude $A \sim 1$cm on the surface of the sail. Such long trains of large and coherent fluctuations in the solar wind are quite unlikely. Thus we conclude that resonant forcing should not be a serious problem.

To gain insight into this result rewrite the expression for the amplitude as

$$\eta \sim \frac{2}{\pi}\left(\frac{U_\varepsilon L}{T}\right)\left(\frac{\Delta\alpha}{\alpha}\right)\left(\frac{\omega_1 t}{2\pi}\right) L$$

Noting that in equilibrium

$$-T\,\frac{\partial^2 \eta_o}{\partial x^2} = U_\nu$$

where U_ν is the photon energy density. Hence by dimensional analysis one has the gross estimate:

$$T \sim \frac{U_\nu L^2}{\eta_o}$$

And therefore

$$\eta \sim \left(\frac{2}{\pi}\right)\left(\frac{U_\varepsilon}{U_\nu}\right)\left(\frac{\Delta\alpha}{\alpha}\right)\left(\frac{\omega_1 t}{2\pi}\right) \eta_o$$

The significant term is $(U_\varepsilon/U_\nu) \lesssim 10^{-3}$ and thus typically many cycles are required before a large oscillation can build up.

So once again we see that the sail does not luff. The dimensionless parameter this time involves the energy density ratio, $(U_\varepsilon L^2/T\eta_o) \sim (U_\varepsilon/U_\nu)$ which is quite small.

Debye Sheath Coupling

An alternative approach to the electrostatic perturbing forces is next examined. Again we consider a membrane perturbed by an external electrostatic force, and hence governed by the wave equation.

$$\rho \frac{\partial^2 \eta}{\partial t^2} - T \frac{\partial^2 \eta}{\partial x^2} = \Delta F$$

This time we take ΔF to be caused by self-consistent perturbations of the Debye sheath. The rippling of the sail perturbs the sheath, which in turn causes perturbing forces to act back on the sail. Hence this calculation is close in spirit to the earlier calculation of gas dynamic coupling. Now, however, we are examining coupling to the plasma Debye sheath.

We take a simple exponential model for the equilibrium sheath. Forces from either side of the membrane add vectorially thus we present the force derivation for a single side and only indicate the result for two sides.

For the front side, $y>0$ one has an equilibrium sheath

$$\phi = \phi_o \exp(-K_d Y) \qquad \text{electrostatic potential}$$

$$E_{yo} = K_d \phi_o \exp(-K_d Y) \qquad \text{electric field}$$

$$\sigma_o = (K_d \phi_o / 4\pi) \qquad \text{surface charge density}$$

where $K_d = (4\pi n_o e^2/T)^{\frac{1}{2}}$

The perturbing force is

$$\Delta F = \Delta\sigma E_{yo} + \sigma_o \Delta E_y$$

where $\Delta E_y = 4\pi\Delta\sigma$ are the perturbed electric field and charge density evaluated at the membrane surface. Note that

$$\Delta E_y = \underset{①}{\frac{\partial E_{yo}}{\partial y}}\ \delta y + \underset{②}{\delta E_y} \qquad , \ \delta y = \eta$$

where term ① represents the contribution to the total perturbed electric field which results from evaluating the equilibrium electric field on the perturbed boundary and term ② represents the perturbed fields evaluated at the equilibrium boundary.

To determine the perturbed fields we need a prescription for the plasma. Again, we note that for times t long compared to an ion transit time through the Debye sheath $\left[\tau_i \sim (\omega_{pi})^{-1} \sim 10^{-6}\text{sec}\right]$, that the quasistatic approximation is valid. In this approximation the potential obeys the Debye equation

$$\nabla^2 \delta\phi - K_d^2 \delta\phi = 0$$

which, for perturbations varying as sin kx on the membrane has the solution

$$\delta\phi = \delta\phi e^{-\sqrt{K^2+K_d^2}\, y} \quad \sin Kx$$

so that $\Delta E_y = 4\pi\Delta\sigma$

$$= -\frac{\partial \delta\phi}{\partial y} + \frac{\partial E_{yo}}{\partial y}\ \delta y$$

$$= \sqrt{K^2+K_d^2}\ \delta\phi - K_d^2 \phi_o \delta y$$

We examine the case of a conducting membrane, which is an appropriate representation of the sail. (For wavelengths>>the sail thickness the two sides of the sail move together and no charging of the dielectric takes place in first order.) Thus we demand that the total potential, which again consists of two terms like ① and ② be zero on the membrane. So one has

$$0 = \frac{\partial \phi_o}{\partial y}\,\delta y + \delta\phi = 0$$

Hence using the equilibrium results one finds that

$$\delta\phi = K_d \phi_o \delta y$$

and so

$$\Delta E_y = \left\{ \sqrt{K^2+K_d^2}\, K_d \phi_o - K_d^2 \phi_o \right\} \delta y$$

The force on one side is thus

$$\Delta F = \left(\frac{K_d^2 \phi_o^2}{2\pi}\right) \left[\sqrt{K^2+K_d^2} - K_d \right] \delta y$$

The total force is obtained by summing the forces acting on the front and back sides. Thus

$$\Delta F = \sum_{f,b} \Delta F \qquad \text{where } f = \text{front},\ b = \text{back}$$

$$= \sum_{f,b} \left(\frac{K_d^2 \phi_o^2}{2\pi}\right) \left[\sqrt{K^2+K_d^2} - K_d \right] \delta y$$

and therefore the wave equation may be written as

$$\rho \frac{\partial^2 \delta y}{\partial t^2} = -TK^2 \delta y + \sum_{f,b} \left(\frac{K_d^2 \phi_o^2}{2\pi}\right) \left[\sqrt{K^2+K_d^2} - K_d \right] \delta y$$

in the long wavelength limit $K<<K_d$ and this reduces to

$$\rho \frac{\partial^2 \delta y}{\partial t^2} = - TK^2 \left\{ 1 - \sum_{f,b} \left(\frac{K_d{}^2 \phi_o{}^2}{4\pi K_d T} \right) \right\} \delta y$$

A plasma which is the same on the front and back will exhibit unstable modes whenever

$$\frac{K_d{}^2 \phi_o{}^2}{2\pi} > K_d T$$

for the solar wind

$$U_\varepsilon = \frac{K_d{}^2 \phi_o{}^2}{4\pi}$$

$$\sim 10^{-7} \text{ergs/cm}^3$$

while

$$U_s = K_d T$$

$$\sim 10^{-4} \text{ergs/cm}^3$$

Thus no instability will occur. Again we find a dimensionless energy ratio which is quite small.

Note again that $T \sim (L^2 U_\nu / \eta_o)$ where η_o is the equilibrium displacement of the sail. Thus the stability parameter can be written as

$$\varepsilon = \frac{K_d{}^2 \phi_o{}^2}{4\pi K_d T} = \left(\frac{U_\varepsilon}{U_\nu} \right) (K_d L)^{-1} \left(\frac{\eta_o}{L} \right) .$$

Each element is this parameter is much less than one thus ε is quite small corresponding to a very stable situation.

Application to Heliogyro

The detailed calculations have used a membrane equation as description of the basic sail. This is adequate for illustrative purposes and is perhaps a reasonable representation of the square sail. A detailed analysis of the heliogyro could be based upon the uncoupled small-motion equations for twist, vertical deflection and inplane deflection. In view of the strong indication that luffing is not a serious problem, which has been derived using the membrane equation, the use of the more elaborate equations seems unjustified. In the event that such analysis were necessary one would again add the electrostatic and gas dynamic forces to the basic equations.

Concluding Comments

These calculations indicate two dimensionless parameters, $\varepsilon_\rho = (n_o m/\rho\alpha)$ the ratio of mass densities and $\varepsilon_u = (U_\varepsilon/U_\nu)$ the ratio of plasma energy density to photon energy density. Both are much less than unity and thus the gas or plasma forces acting upon the sail are much less than the forces caused by photon pressure. No mechanism has been found which would significantly amplify the impact of the plasma forces thus no instabilities develop.

7. INDUCTION CURRENT AND INDUCTION FORCE

When a conducting satellite moves through a stationary magnetized plasma an electric field $\vec{E} = -\frac{V \times B}{c}$ is set up within it, due to the polarization of the free charge produced by the motion perpendicular to B [1,2], Figure 7.1. Likewise since B field lines can be regarded as frozen into the solar wind plasma motion of the solar wind plasma past the satellite with velocity V_s produces the field $\vec{E} = \frac{\vec{V}_s \times \vec{B}}{c}$. The potential variation on the satellite surface causes electrons to land preferentially on the more positive portions, and protons to land preferentially on the more negative portions. Also photo-electrons emitted from the positive parts are more likely to be attracted back to the surface.

This situation causes a steady current to flow through the satellite. The current is calculated by using the potential at each point on the surface to calculate the plasma current into the satellite. The potential is a linear function of the dimension x in the $\vec{V}_s \times \vec{B}$ direction. The requirement that the net current into the satellite equal the net current out of the satellite gives the potential. The possible consequences of this current in our view are twofold, the current crossed with the magnetic field produces forces and torques, and the current dissipates energy in the aluminum sail film. We shall argue that the induction forces

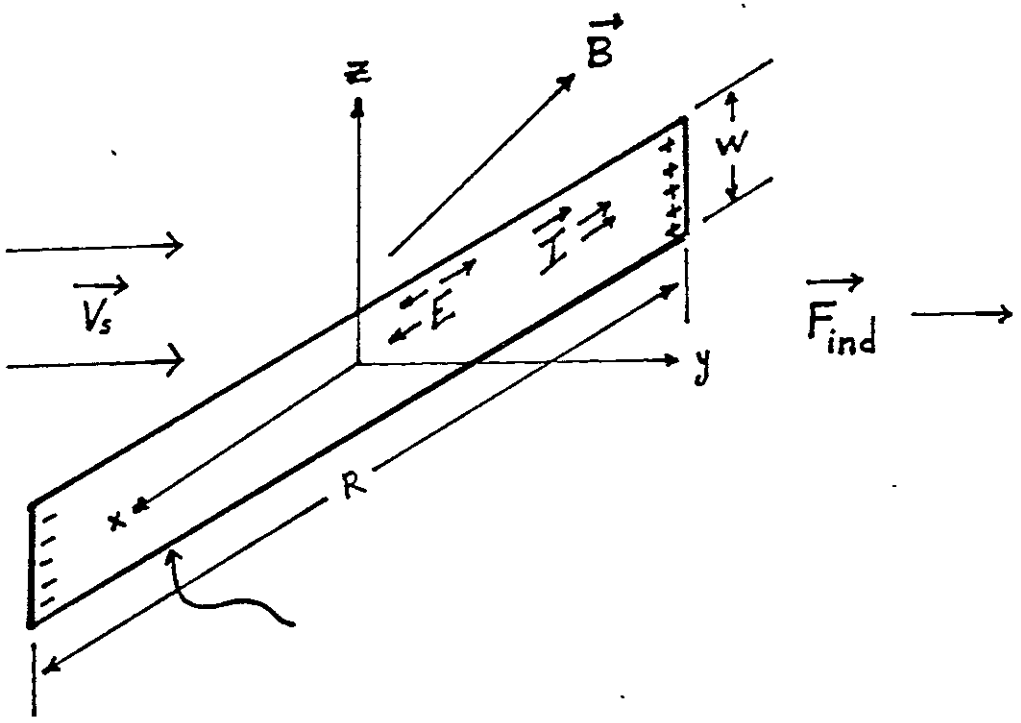

Figure 7.1. Induction geometry.

are far smaller than the radiation pressure, and that the energy dissipated by conduction is negligible in comparison to the sunlight energy absorbed by the aluminum.

It is not necessary to perform a detailed calculation to show that the above effects are small. Figure 7.2 shows the general situation with the currents. For this diagram we assumed that the potential changes sign somewhere along the blade. This is not necessarily true. The net current per unit area into or out of the sail at any point x is given by the sum $\Gamma(x)$ of the three fluxes at that point. A crude bound on the maximum current along the sail can be made by taking the largest of the three current densities $\frac{J_{ph}}{e} = \Gamma_{ph} = 2.6 \times 10^{11}/cm^2$- ser (at .3 a.u.). multiplying by the electronic charge and one half the area and assuming this current flows in one half the blade and out the other half. This current is

$$I_{max} = \tfrac{1}{2} e \Gamma_{ph} \cdot (w=8\times10^{2}cm)(R=6.24\times10^{5}cm) = 3.12\times10^{10} esu/sec,$$

$$I_{max} = 10.5 \text{ amp.}$$

This total current multiplied by the length and magnetic field and divided by the blade area gives a value for the total induction force per unit area

$$F = \frac{I_{max} \cdot R \cdot (B=58\times10^{-5}gauss)}{c \cdot R \cdot w},$$

$$F = 7.54 \times 10^{-7} dyne/cm^2.$$

This is about .15% of the solar radiation pressure at .3 a.u. and thus seemingly negligible.

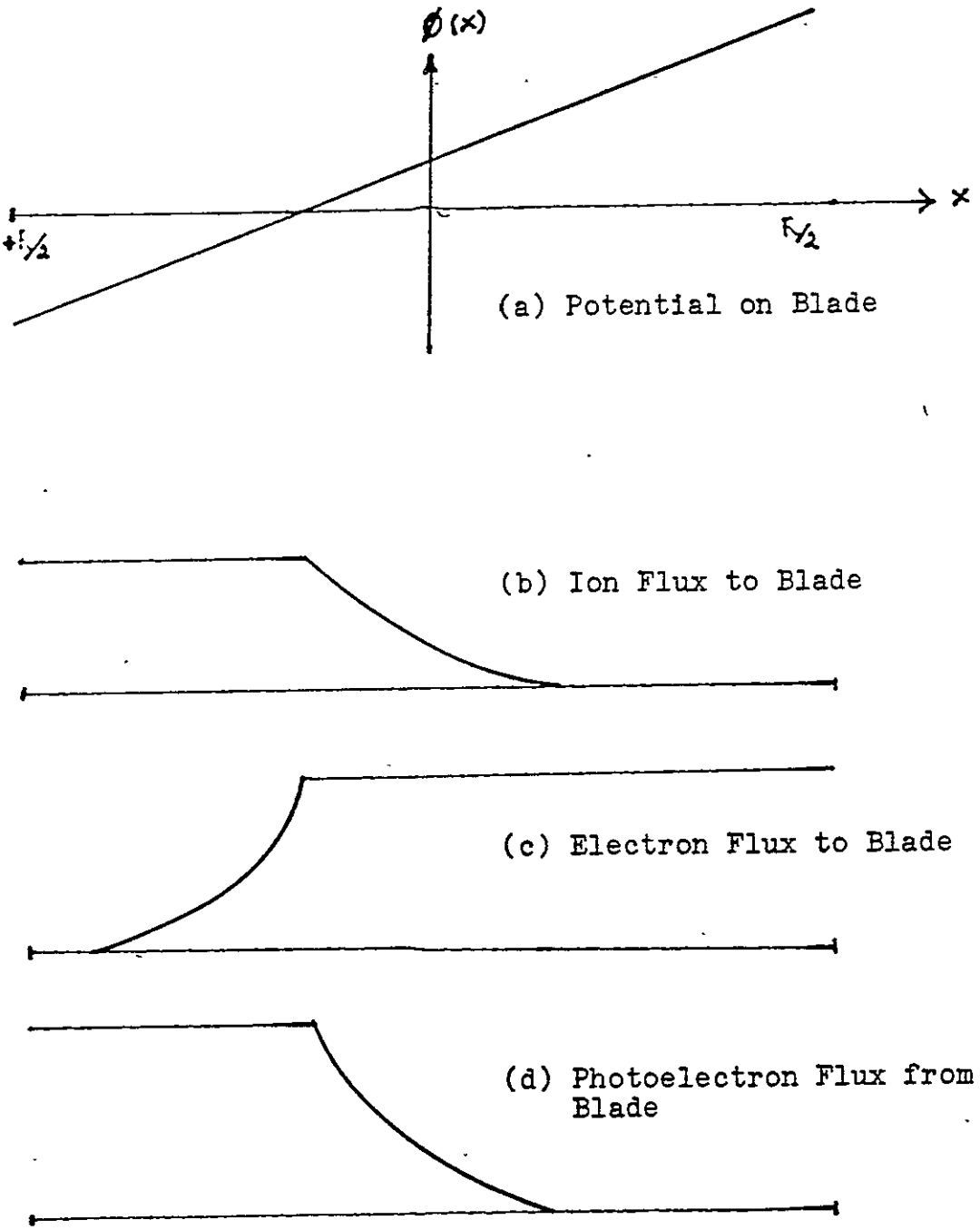

Figure 7.2. Sail potential and particle fluxes.

The current density in the VDA implied by I_{max} is

$$J = \frac{I_{max}}{w(t=1000\text{Å})} = 3.9 \times 10^{12} \text{esu/cm}^2\text{-sec} .$$

Using the approximate value for the conductivity at 525°K $\sigma \sim 2.6 \times 10^{17} \text{sec}^{-1}$ we find the volume energy deposition rate

$$\frac{dw}{dt} = \frac{J^2}{\sigma} = 5.85 \times 10^7 \frac{\text{erg}}{\text{cm}^2\text{-sec}} = 5.85 \text{ watt/cm}^3.$$

This implies a per unit area energy absorption of 5.85×10^{-5} watt/cm^2. The VDA absorbs about 10% of the incident optical energy, or at 0.3 a.u. about 0.14 watt/cm^2. Thus the induction current should not affect the thermal balance of the sail.

In Section 9 we point out that the induction current might possibly interfere with magnetic field measurements.

8. EFFECTS OF SOLAR SAIL OPERATION ON THE PAYLOAD

In this section we consider the effects of the presence of the solar sail on the operation of the payload itself. The possible areas of concern are

1) Safety

2) Effects on particle measurements,

3) Effects on field measurements

4) Electromagnetic Interference (EMI).

We will not consider the possible effects on various optical observations since this will depend on the specific configuration. We do note however that the periodic illumination of various parts of the payload by the rotating blades could cause spurious readings. Likewise light scattered from matter emitted from the sail could influence readings of very low light intensity measurements.

In the proposed configuration, the payload is asymetric about the sail spin axis. Further, one part of the payload is shielded from the sun with a large shade. Several aspects of this proposed configuration could have serious effects on the operation of the scientific instruments as well as perhaps presenting a hazardous situation.

Safety. Because the payload part of the solar sail vehicle is probably composed of materials with different surface characteristics from the sail itself, the equilibrium electrostatic potential that it would assume in the undisturbed medium could differ considerably from that assumed by the sail. If the ground between them depended on a potentially intermittant connection through the despin mechanism, then discharges could occur with large currents being injected into the payload proper. Therefore we emphasize the need for making firm connections between spacecraft chassis ground and the sail. The current through this joint should be of the order of a few tens of microamperes and be more or less constant.

The alternative of completely isolating the payload seems to be less desirable for several reasons. It would make communication between the parts more difficult (i.e. optical couplers needed), and the varying differential potentials would affect adversely particle measurements while the payload is still attached to the sail.

Effects on Particle Measurements. The presence of the solar sail can influence the attempts to measure the particles in the undisturbed plasma in several ways:

1) Production of extraneous particles
2) Creation of local electric fields, and
3) Creation of local magnetic fields.

As has been discussed in other sections of this report, the sail will produce copious amounts of photoelectrons, back-scattered electrons, and secondary electrons. Smaller amounts of neutral particles and positive ions are also produced. In the most likely charge state, the total spacecraft will also accelerate (by the potential of the whole structure) either the electrons or ions while retarding the other species. Since there is most likely no way to eliminate all of these effects, the experimenters will be forced to design instruments which operate in the sail environment. For instance, an instrument designed to measure low energy (less than 20 eV) electrons in the vicinity of a comet will risk excessive counts on its sensors if operated for long periods in the cruise mode. Therefore the instrument must have command modes available to avoid this energy range during cruise, or only be operated for short test periods.

As has been shown by Whipple[1] using data from ATS-6, careful analysis of particle data as a function of energy and angle with respect to the spacecraft coordinates can allow the

experimenter to deconvolve the effects of local electric fields and thus sort out many of the locally produced particles from the natural ones. However this analysis is time consuming and costly.

No algorithm for this kind of study has yet been developed for the solar sail, but the nature of the heliogyro might simplify the work somewhat because of the periodic modulations to be expected as the gyro rotates.

Creation of local electric fields by the sail will distort the trajectories of the incoming ambient particles. These fields are also responsible for reflecting the locally produced particles back on paths which allow them to be counted by the payload instruments. As was alluded to above, some mapping of these fields can be accomplished by studying the measured distribution function of all particles reaching a given detector. This might be the only way to measure such fields if long booms cannot be deployed from the payload before jettisoning the sail. (We do not consider here the interesting posibility that the gyro blades themselves can be used as electric field probes.)

These locally produced fields will most likely consist of an overall charge, a potential minimum produced in the plasma sheath, and localized irregular fields due to differential charging. But to this list we must add another possible

candidate due to the proposed configuration. The various optical sensors are shielded from the sun by a large shade. This will cause dielectrics in the area (such as the lenses themselves) to charge more negatively than the main body. However light reflecting from the blades of the gyro as they rotate under this section can produce enough photoelectrons to discharge the dielectrics periodically. This could produce a large modulation on local electric fields which would be very difficult to untangle in the particle data. Similar comments can be made about any shadowed portion of the payload, but this effect is surely heightened by the presence of the sun shade.

As disruptive as these effects will probably be on particle measurements, the effects of locally produced magnetic fields might be worse. If we assume an induction current in the blade of the order of 10 amperes (see Section then we can easily estimate the magnetic field to be expected at the instrument aperture due to this contaminant. For probable dimensions, the induced magnetic field is in the order of hundreds of gammas (10^{-5}gauss = 1 gamma). In the solar wind the undisturbed field in typically of the order of gammas or less.

The effect of this field will not be noticable on most ions or on electrons of more than a few hundred electron volts energy. However, the lower energy electrons will have their trajectories so distorted that one might not be able to deconvolve the bending the underwent in this magnetic field.

Naturally, this problem can be solved much more easily than the problem of the stray electric fields. All one has to do is to prevent the existance of such large currents near the payload. This should be possible without compromising other mission objectives.

Effects on Field Measurements. Of necessity, local field contamination has been discussed in the previous section on particle measurements. All that needs to be said here is that deployment of long electric antennae is not advisable in the presence of the solar sail. Even stub booms might be saturated a large fraction of the time.

The example of the possible levels of magnetic contamination given in the previous section shows that a magnetometer on the payload would have a difficult time indeed trying to measure natural fields in the presence of a periodically varying field which is potentially orders of magnitude greater than the desired signal.

Electromagnetic Interference. EMI induced in the payload by the solar sail is a possible hazard in addition to the obvious safety aspects. Excessive noise could trigger counters, upset logic, etc. However, at this time we have been unable to isolate any aspect of the solar sail itself which would produce excessive EMI, providing that the grounding and sail shorting is carefully done.

9. EXPERIMENTAL PROGRAM

Even though most of the analysis done in this report indicate that possible sail-plasma interactions are an order of magnitude or more smaller than other interactions, an experimental program should be undertaken to verify the various results.

It would be beyond the scope of this study to prepare a complete experimental program here, but a similar program that might be of use to the study of the solar sail has been prepared by MAYA for NASA Lewis Research Center under a subcontract to Systems, Science, and Software (S^3) of La Jolla.[1] The purpose of the report was to develop plans for the experiments which must be conducted in order to verify the ground test mathematical model (GTMM) of spacecraft charging which has been developed by S^3 for Lewis Research Center.

Special problems that involve testing of the sail involve its size. For instance, electrical-mechanical oscillations might not scale linearly, and testing a full-sized blade is not feasible.

Therefore we suggest that the best policy is to test as large samples as possible by placing them in high-vacuum systems with appropriate irradiation by particles and photons. While close watch should be kept for induced mechanical effects, the prime observations should be the leakage current

and induced potentials. Simultaneously EMI produced from sporadic breakdowns should be monitored to give an idea of what might be expected in orbit. Because of the very thin material used, large potentials cannot be generated before breaking down. Therefore we expect much less spectacular displays with solar sail material than has been seen in similar tests at Lewis on normal spacecraft materials.

Contamination of the environment probably cannot be estimated accurately from ground tests since the interactions with the vacuum system itself will also contribute extraneous particles.

Some attempt should be made to assess the lifetime of the sail in simulated solar wind conditions. We have not attempted to assess the impact of induced sputtering or the effects of cross-linking of the polymers by radiation, but these and other effects which are indirectly related to the natural environment could combine to shorten the expected lifetime on orbit.

Finally, we strongly recommend that anattempt be made to simulate the deployment of a sail blade under as realistic conditions as possible. As can be seen from Section 5 on deployment, there is much more than first meets the eye about possible problems in unrolling this very thin membrane. Even when the front and back surfaces are shorted together, there

might be some net force induced by the environment. As in the previous case, scaling here is difficult. The expected forces are quite small, but might be significant. A possible observation would be discharges at the separation line.

SYMBOLS		PAGE
r	Distance From Sun	3-1
V	Solar Wind Velocity	3-1
n	Solar Wind Number Density	3-2
T	Solar Wind Average Temperature	3-6
T_e	Solar Wind Electron Temperature	3-7
R_T	Temperature Ratio	3-8
N_c	Cold Number Density	3-8
N_H	Hot Number Density	3-8
f_e	Electron Distribution Function	3-9
f_m	Maxwellian Distribution Function	3-9
$\mathcal{V}_s$	Solar Sail Potential	4-2
m_e	Electron Mass	4-3
m_p	Proton Mass	4-3
v_e	Electron Thermal Velocity	4-3
v_p	Proton Thermal Velocity	4-3
b	Cavity Length	4-3
w	Sail Width	4-3
Γ_e	Electron Number Flux	4-6
f_p	Proton Distribution Function	4-11
Γ_p	Proton Number Flux	4-11
ϕ	Dimensionless Sail Potential	4-11
Γ_{ph}	Photon Number Flux	4-14
$S(E)$	Secondary Electron Yield	4-15
$i^5\mathrm{erfc}(z)$	Iterated Error Function	4-15
σ	Conductivity	4-17
J_σ	Current Density	4-17
θ	Angle Between Solar Wind Flow Direction and Solar Sail Surface Normal	4-24
Q	Total Charge	5-6
I	Total Current	5-6
τ	Radiation Pressure Torque	5-7
P_s	Radiation Pressure	5-7
η	Solar Sail Mass Per Unit Length	5-9
ε	Dielectric Permittivity	6-4

SYMBOLS		PAGE
dsk	Variation in Kapton Thickness	6-4
dk	Kapton Thickness	6-4
dsv	Variation in VDA Thickness	6-4
dv	VDA Thickness	6-4
dew	Loose Wrap Distance	6-4
ω	Characteristic Frequency of Oscillation	7-4
T	Tension in Membrane	7-4
ρ	Density of Membrane	7-4
C_s	Sound Speed	7-4
η	Displacement of Sail Surface	7-5
ϕ	Electrostatic Sheath Potential	7-14
ϕ_o	Electrostatic Surface Potential	7-14
σ_o	Surface Charge Density	7-14
E_y	Sheath Electric Field	7-14
E_{yo}	Surface Electric Field	7-14
$\delta 0$	Perturbe Sheath Potential	7-15
$\vec{E}$	Plasma Electric Field	8-1
$\vec{V}$	Plasma Flow Velocity	8-1
$\vec{B}$	Magnetic Field Vector	8-1
c	Speed of Light	8-1
F	Force per Unit Area	8-3

REFERENCES

SUMMARY

No references.

1. INTRODUCTION

No references.

2. THE SOLAR WIND ENVIRONMENT

1) M. Montgomery, S. Bame, A. Hundhausen, J. Geophys. Res., 73, 1968, p. 4999.

2) A. Hundhausen, S. Bame, J. Ashbridge, S. Sydoriak, J. Geophys. Res., 75, 1970, p. 4643.

3) W. Feldman, J. Ashbridge, S. Bame, M. Montgomery, S. Gary, J. Geophys. Res. 80, 1975, p. 4181.

4) P. Sturrock, R. Hartle, Astrophys. Jour., 151, 1968, P. 1155.

5) H. Rosenbauer, H. Miggeniender, M. Montgomery, R. Schwen, in Physics of Solar Planetary Environments, Vol. 1, Proceedings of the International Symposium on Solar-Terrestrial Physics, 1976, p. 319.

6) T. Suess, in Ref. 5.

3. SAIL CHARGING IN THE SOLAR WIND

1) Alpert, J., Gurevich, A., Pitaevskii, L., Space Physics with Artificial Satellites, Consultants Bureau, New York, 1965.

2) Alpert, J., Waves and Satellites in the Near Earth Plasma, Consultants Bureau, New York, 1974.

3) Gurevich, A., Pitaevskii, L., Smirnova, V., Space Sci. Rev. 2, p. 680, 1963.

4) Parker, L., Computation of Collisionless Steady State Plasma Flow Past a Charged Disc., NASA CR-144159, Lee Parker Inc., Feb. 1976.

5) Liu, V., Space Sci. Rev. 9, p. 423, 1969.

6) Martin, A., Planet Space Sci. 22, p. 121, 1974.

7) Gurevich, A., Pitaevskii, L., Phys. Rev. Lett. 15, p. 346, 1965.

8) Grard, R., Jour. Geophys. Res. 78, p. 2885, 1973.

9) Katz, I., Parks, D., Wilson, A., Three Dimensional Dynamic Study of Electrostatic Charging in Materials, Interim Report. NAS 3-20119, NASA Lewis Research Center, Jan. 1977.

10) Grard, R., Knott, K., Pederson, A., in Photon and Particle Interactions with Surface in Space, p. 163, Ed. R. Grard, D. Reidel Publ. Co. 1973.

11) Purvis, C., Stevens, N., Oglebay, J., Charging Characteristics of Materials: Comparison of Experimental Results with Simple Analytic Models, NASA TM-73606, Lewis Research Center, 1976.

4. USE OF THE SOLAR SAIL IN THE NEAR EARTH ENVIRONMENT

1) Richard H. MacNeal, MacNeal-Schwendler Corporation, private communication.

2) Jerry Wright, JPL Mission Analysis, private communication.

3) A. Rosen, "Large Discharge and Arcs on Spacecraft", Astronautics and Aeronautics, June 1975.

4) Spacecraft Charging by Magnetospheric Plasmas, A. Rosen Ed., MIT Press, 1976.

5) M. Kaminsky, Atomic and Ionic Impact Phenomena on Metal Surfaces, p. 176, 232, Springer-Verlag, 1965.

6) Richard H. MacNeal, NASA-JPL Presentation Summary, March 7, 1977.

5. DEPLOYMENT PROBLEMS DUE TO STATIC ELECTRICITY

1) William Caroll, JPL private communication.

2) Richard H. MacNeal, "Heliogyro Fundamentals", MacNeal-Swindler Co.

3) Handbook of Chemistry and Physics. Chemical Rubber Publishing Co.

4) L. I. Maissel, An Introduction to Thin Films. Gordon and Breach, 1973, p. 258.

5) Leonard B. Locb, Static Electrification Springer-Verlag, 1958.

6) W. R. Harper, Contact and Frictional Electrification, Oxford University Press, 1967.

7) I. Giaever and J. C. Fisher, J. Appl. Phys. 32, 1961, p. 172.

8) I. Giaever and K. Megerle, Phys. Rev. 122, 1961, p. 1101.

6. ELECTROMECHANICAL OSCILLATIONS OF THE SOLAR SAIL

1) Morse and Ingard, Theoretical Acoustics, New York, McGraw Hill, 1968.

7. INDUCTION CURRENT AND INDUCTION FORCE

1) Drell, S., Foley, H., and Ruderman, M., J. Geophys. Res. 70, 1965, p. 3131.

2) Chu, C. K., Gross, R., AIAA Jour. 4 1966, p. 2209.

8. EFFECTS OF THE SOLAR SAIL OPERATION ON THE PAYLOAD

No references.

9. EXPERIMENTAL PROGRAM

1) LaQuey, R. E. "Experimental Plan for the Testing of Space-craft Charging Models" MAYA Development Corporation - Final Report Subcontract S-5087 to Systems, Science and Software Prime Contract NAS3-20119.

DISTRIBUTION LIST

National Aeronautics and Space Administration Washington, D.C. 20546	
ATTN: W. R. Hudson/Code RP	1 copy
D. P. Cauffman/Code ST	1 copy
A. F. Timothy/Code ST	1 copy
National Aeronautics and Space Administration Ames Research Center Moffett Field, CA 94035	
ATTN: H. Lum, Jr./M.S. 244-7	1 copy
National Aeronautics and Space Administration Goddard Space Flight Center Greenbelt, MD 20771	
ATTN: R. O. Bartlett/Code 408.0	1 copy
A. Kampinsky/Code 715.0	1 copy
E. G. Stassinopoulos/Code 601.0	1 copy
Jet Propulsion Laboratory 4800 Oak Grove Drive Pasadena, CA 91103	
ATTN: R. Goldstein/M.S. 122-123	1 copy
National Aeronautics and Space Administration Lyndon B. Johnson Space Center Houston, TX 77058	
ATTN: J. E. McCoy/Code TN2	1 copy
National Aeronautics and Space Administration Langley Research Center Hampton, VA 23665	
ATTN: J. D. DiBattista/M.C. 158B	1 copy
National Aeronautics and Space Administration Lewis Research Center 21000 Brookpark Road Cleveland, OH 44135	
ATTN: Head, Contract Section B/M.S. 500-313	1 copy
Technical Utilization Office/M.S. 7-3	1 copy
Report Control Office/M.S. 5-5	1 copy
Office of Reliability and Quality Assurance/M.S. 500-211	1 copy
AFSC Liaison Office/M.S. 501-3	2 copies
Library/M.S. 60-3	2 copies
J. C. Roche/M.S. 501-8	20 copies

DISTRIBUTION LIST (Continued)

National Aeronautics and Space Administration
George C. Marshall Space Flight Center
Marshall Space Flight Center, AL 35812
ATTN: C. R. Baugher/ES 53 — 1 copy

National Aeronautics and Space Administration
Scientific and Technical Information Facility
P. O. Box 8757
Baltimore/Washington International Airport
Maryland 21240
ATTN: Accessioning Department — 10 copies

Air Force Geophysics Laboratory
Hanscom Air Force Base, MA 01731
ATTN: PH/C. P. Pike — 1 copy

Air Force Materials Laboratory
Wright-Patternson Air Force Base, OH 45433
ATTN: MBE/W. Lehn — 1 copy

Air Force Office of Scientific Research
Bolling Air Force Base
Washington, D. C. 20332
ATTN: H. R. Radoski/NP — 1 copy

Air Force Systems Command
AFSC/DLCEA
Andrews Air Force Base, MD 20331
ATTN: Captain D. L. Beadner — 1 copy

Air Force Weapons Laboratory
Kirtland Air Force Base, NM 87117
ATTN: ELC/Major M. T. Barnett — 1 copy

Space and Missile Systems Organization
Los Angeles AF Station
P. O. Box 92960
Worldway Postal Center
Los Angeles, CA 90009
ATTN: YATT/Captain M. Bunn — 1 copy

DISTRIBUTION LIST (Continued)

Defense Nuclear Agency Headquarters
Washington, D.C. 20305
ATTN: RAEV/Lt. Colonel T. Hawranick — 1 copy

Communications Research Centre
Shirley Bay
P. O. Box 490, Station A
Ottawa, Ontario
Canada KIN 8T5
ATTN: V. Gore — 1 copy

Department of Electrical Engineering
Pennsylvania State University
121 Electrical Engineering
East Building
University Park, PA 16802
ATTN: J. Robinson — 1 copy

Department of Physics
University of California at San Diego
P. O. Box 109
La Jolla, CA 92037
ATTN: C. McIlwain — 1 copy

Aerojet Electrosystems Company
1100 West Hollyvale Street
Azusa, CA 91720
ATTN: C. Fischer/Dept. 6751 — 1 copy

Aerospace Corporation
P. O. Box 92957
Los Angeles, CA 90009
ATTN: J. R. Stevens — 1 copy

Boeing Aerospace Company
P. O. Box 3999
Seattle, WA 98124
ATTN: H. Liemohn/M.S. 8C-23 — 1 copy

Communications Satellite Corporation
Comsat Laboratories
Clarksburg, MD 20734
ATTN: A. Meulenberg, Jr. — 1 copy

DISTRIBUTION LIST (Continued)

Ford Aerospace and Communications Corporation
Western Development Laboratories Division
3939 Fabian Way
Palo Alto, CA 94303
ATTN: D. M. Newell/M.S. G-80 — 1 copy

General Electric Company
Valley Forge Space Center
P. O. Box 8555
Philadelphia, PA 19101
ATTN: V. Belanger/U-2439 — 1 copy

Grumman Aerospace
Bethpage, NY 11714
ATTN: M. Stauber — 1 copy

Hughes Aircraft Company
P. O. Box 92919
Los Angeles, CA 90009
ATTN: E. Smith/M.S. A620 — 1 copy

IRT Corporation
P. O. Box 80817
San Diego, CA 92138
ATTN: J. Wilkenfeld — 1 copy

JAYCOR
1401 Camino del Mar
Del Mar, CA 92014
ATTN: E. P. Wenaas — 1 copy

Kaman Science
1500 Garden of the Gods Road
Colorado Springs, CO 80907
ATTN: F. Rich — 1 copy

Lee W. Parker, Inc.
252 Lexington Road
Concord, MA 01742
ATTN: L. Parker — 1 copy

Lockheed Palo Alto Research Laboratory
3251 Hanover Street
Palo Alto, CA 94303
ATTN: J. B. Reagan/Bldg. 205, Dept. 52-12 — 1 copy

Martin Marietta Corporation
P. O. Box 179
Denver, CO 80201
ATTN: D. E. Hobbs — 1 copy

Massachusetts Institute of Technology
Lincoln Laboratory
P. O. Box 73
Lexington, MA 02173
ATTN: F. G. Walther — 1 copy

McDonnell Douglas Astronautics Company
5301 Bolsa Avenue
Huntington Beach, CA 92647
ATTN: W. P. Olson — 1 copy

Mission Research Corporation
1150 Silverado Street
P. O. Box 1209
La Jolla, CA 92038
ATTN: V. van Lint — 1 copy

RCA Astroelectronics Division
P. O. Box 800
Princeton, NJ 08540
ATTN: H. Strickberger/M.S. 91 — 1 copy

Science Applications, Inc.
101 Continental Building
Suite 310
El Segundo, CA 90245
ATTN: D. McPherson — 1 copy

Science Applications, Inc.
2860 S. Circle Drive
Colorado Springs, CO 80906
ATTN: E. E. O'Donnell — 1 copy

DISTRIBUTION LIST (Continued)

Simulation Physics, Inc.
41 B Street
Burlington, MA 01803
ATTN: R. G. Little — 1 copy

Stanford Research Institute
333 Ravenswood Avenue
Menlo Park, CA 90425
ATTN: J. Nanevicz — 1 copy

TRW Systems
One Space Park
Redondo Beach, CA 90278
ATTN: A. Rosen — 1 copy